A Photometric Study of the Outer Halo Globular Cluster NGC 5824

A. R. Walker[1], G. Andreuzzi[2], C. E. Martínez-Vázquez[3,4], A. M. Kunder[5,10], P. B. Stetson[6],
S. Cassisi[7], M. Monelli[3,4], G. Bono[8], M Dall'Ora[9], and A. K. Vivas[1]

[1] Cerro Tololo Inter-American Observatory, National Optical Astronomy Observatory,
Casilla 603, La Serena, Chile; awalker@ctio.noao.edu
[2] Fundación Galileo Galilei—INAF, Breña Baja, La Palma, Spain
[3] Instituto de Astrofísica de Canarias, Calle Via Lactea, E-38205, La Laguna, Tenerife, Spain
[4] Universidad de La Laguna, Dpto. Astrofísica, E-38206, La Laguna, Tenerife, Spain
[5] Leibniz-Institute für Astrophysik Potsdam (AIP), Ander Sternwarte 16, D-14482, Potsdam, Germany
[6] Dominion Astrophysical Observatory, Herzberg Institute of Astrophysics, National Research Council,
Victoria, British Columbia V9E 2E7, Canada
[7] INAF-Osservatorio Astronomica di Collurania, via M. Maggini, I-64100 Teramo, Italy
[8] Departimento di Fisica, Universitá di Roma Tor Vergata, via della Ricerca Scientifica 1, I-00133, Rome, Italy
[9] INAF-Osservatorio Astronomica di Capodimonte, salita Moiariello 16, I-80131, Napoli, Italy
[10] Saint Martin's University, Old Main, 5000 Abbey Way SE, Lacey, WA 58903, USA
Received 2017 April 17; revised 2017 May 11; accepted 2017 May 11; published 2017 June 13

Abstract

Multi-wavelength CCD photometry over 21 years has been used to produce deep color–magnitude diagrams (CMDs) together with light curves for the variables in the Galactic globular cluster NGC 5824. Twenty-one new cluster RR Lyrae stars are identified, bringing the total to 47, of which 42 have reliable periods determined for the first time. The CMD is matched using BaSTI isochrones with ages of 13 Gyr, and reddening is found to be $E(B-V) = 0.15 \pm 0.02$; using the period–Wesenheit relation in two colors, the distance modulus is $(m-M)_0 = 17.45 \pm 0.07$ corresponding to a distance of 30.9 Kpc. The observations show no signs of populations that are significantly younger than the 13 Gyr stars. The width of the red giant branch does not allow for a spread in [Fe/H] greater than $\sigma = 0.05$ dex, and there is no photometric evidence for widened or parallel sequences. The V, c_{UBI} pseudo-CMD shows a bifurcation of the red giant branch that by analogy with other clusters is interpreted as being due to differing spectral signatures of the first (75%) and second (25%) generations of stars whose age difference is close enough that main-sequence (MS) turnoffs in the CMD are unresolved. The cluster MS is visible against the background out to a radial distance of ~17 arcmin. We conclude that NGC 5824 appears to be a classical Oosterhoff Type II globular cluster, without overt signs of being a remnant of a now-disrupted dwarf galaxy.

Key words: Galaxy: stellar content – stars: distances – stars: evolution – stars: horizontal-branch – stars: Population II

1. Introduction

NGC 5824 (C1500-328) is an outer halo globular cluster (GC) that until recently has received little attention, at least in part due to the combination of its considerable distance from the Sun and a high central concentration. Together these make ground-based observations of individual stars difficult. A visual inspection by Innes (1925) refers to the cluster as being very condensed, and the Harris (1996) database lists a central luminosity of $4.1 \times 10^4 L_\odot$ per cubic parsec, ranking in the highest 20% of Galactic GCs. Harris (1996) shows that after NGC 2419, NGC 5824 is the most massive GC more distant than 20 kpc from the Galactic center, and it is the fourteenth most luminous GC in the Galaxy. NGC 5694 and NGC 6229 are two clusters at similar distances from the Galactic center, but are a factor of two to three less luminous than NGC 5824.

With Galactic coordinates $l = 332°.56$, $b = 22°.07$ the foreground star contamination from the Galactic bulge is substantial; however, the reddening is moderate, with $E(B-V) = 0.13$ (Zinn 1985) or $E(B-V) = 0.15$ (Schlafly & Finkbeiner 2011), assuming $R = 3.1$ in each case. Kinman (1959) found a spectral type of F5, thus NGC 5824 is metal-poor. This result has been confirmed by more recent work, in particular, Da Costa et al. (2014), who derive a metallicity of [Fe/H] $= -2.01 \pm 0.13$ from spectroscopy of the calcium triplet (CaT) absorption lines,

and Roederer et al. (2016) who in a high-resolution spectroscopic study of 26 bright red giant branch (RGB) stars found that [Fe/H] $= -1.94 \pm 0.02$ (statistical) ± 0.10 (systematic), using Fe II lines. In addition Roederer et al. (2016) find no evidence for variation in [Fe/H] at the 0.08 dex level in their sample of stars, noting that the stars for which Da Costa et al. (2014) found a small dispersion were a fainter group than the 26 bright RGB stars that are common to both investigations. However, Roederer et al. (2016) find an internal dispersion of 0.28 dex in [Mg/Fe] and point out that this behavior is observed in several other luminous, metal-poor clusters. Two stars of their sample were observed with *Magellan* MIKE and show the expected correlation of [Mg/Fe] with [O/Fe], and anti-correlation of [Mg/Fe] with [Na/Fe] and [Al/Fe]. So although the light-element observations for a substantial sample of stars in NGC 5824 are still lacking, it may be possible to use the [Mg/Fe] measurements as a proxy to split the first and second generation stars. Roederer et al. (2016) also find that a single star of their sample shows substantial s-process enhancement; for the other 25 stars, they state that n-capture abundance patterns are essentially identical and consistent to those for field stars with equivalent stellar parameters and metallicities.

The first color–magnitude diagram (CMD) for NGC 5824 was photographic (Harris 1975) and only just reached to the horizontal branch (HB); however, the data were of sufficient

quality that 10 RR Lyrae variable stars (RRL) could be measured photometrically, resulting in a distance of 25 kpc from the Sun by adopting $M_V(\text{HB}) = 0.6$. It was noted from the slope of the RGB that the cluster appeared to be metal-poor with a possible blue horizontal branch (BHB). This was confirmed in the first comprehensive photometric study of NGC 5824, where Cannon et al. (1990) used a small-format CCD to measure 285 stars to $V = 20.5$. Assuming a reddening $E(B - V) = 0.13$, they found an apparent modulus of 18.0 ± 0.2 mag and a color for the RGB at the level of the HB of $(B - V)_{0,g} = 0.77$ corresponding to $[\text{Fe/H}] = -1.7$, and confirmed that the cluster has a well-populated BHB. A deeper CMD to $V \sim 22$ by Brocato et al. (1996) showed a possible extreme BHB component (EHB stars) and, while demonstrating some photometric calibration differences with Cannon et al. (1990), derived rather similar cluster parameters, finding from $V_{\text{HB}} = 18.45 \pm 0.05$ and $(B - V)_{0,g} = 0.73 \pm 0.03$ that $[\text{Fe/H}] = -1.85$, adopting the Zinn (1985) reddening. A relatively shallow *HST B* and *V* CMD (Piotto et al. 2002) shows no non-canonical sequences, and neither did the analysis of archival *HST* observations by Sanna et al. (2014).

Study of NGC 5824 languished between 1995 and 2008, though several investigators using NOAO and ESO telescopes observed the cluster photometrically in this period; these images can be found in the relevant archives, and are part of the present analysis. During the same period there was a paradigm shift for globular clusters, with the discovery of association between some clusters and dwarf galaxies past and present, and with many of the more massive clusters in particular demonstrating a variety of non-canonical behavior such as metallicity spreads and/or multiple populations (see, e.g., Piotto 2009; Gratton et al. 2012; Milone et al. 2013; Renzini et al. 2015). In this context, Newbury et al. (2009) pointed out the possible association of NGC 5824 with the Cetus Polar Stream, for which Pawlowski et al. (2012) find an orbit almost perpendicular to the northern-sky Disk of Satellites, part of the Vast Polar Structure of satellite galaxies, globular clusters and streams discussed by these authors. Law & Majewski (2010) exclude NGC 5824 from any association with the Sagittarius dwarf galaxy that is presently colliding with the Milky Way. Notably, Grillmair et al. (1995) included NGC 5824 in their wide-field photographic study searching for tidal tails around a sample of 12 globular clusters. They demonstrate the good fit of a power law with exponent -2.2 ± 0.1 over the whole range of radius out to a nominal $r = 45$ arcmin, though the high stellar background means that error bars are large for the outer data points (those with $r > 13$ arcmin). Indeed, later work by Carballo-Bello et al. (2012) shows evidence for a profile truncation starting at about 10 arcmin, and Carballo-Bello et al. (2014) find no associated extra-tidal structure; however, see the discussion by Da Costa et al. (2014) in the context of NGC 5824 as being the remnant of a dwarf galaxy that was accreted by the Milky Way several gigayears ago and is now disrupted. An independent study of the structural properties of 26 GC using a combination of *HST* and ground-based imaging (Miocchi et al. 2013) fits King and Wilson models to NGC 5824, the limiting radii derived are very different, 8.79 and 40 arcmin respectively.

In this paper, we present a deep and accurate CMD, reaching to $V \sim 24$ from extensive observations on several telescopes over more than two decades, that we compare to BaSTI (Pietrinferni et al. 2004, 2013) isochrones. The data set includes observations in *UBVRI* filters, albeit with many fewer

U and *R* observations. A few observations were made in other filters and these have been transformed as described below. We have increased the number of variable stars to 59, of which 47 appear to be RRL cluster members, with in addition one certain and another probable Type II Cepheid, four SX Phe stars, and five eclipsing binaries. An additional RRL appears to be a very distant halo field star that happens to be in the field of view of NGC 5824. We have derived positions and mean photometry for all of them, and periods for all except six stars; though a few of these 53 periods are marked (Appendix) as not being reliable. We subsequently calculated light-curve parameters for the RRL in order to help elucidate the nature of NGC 5824.

The arrangement of this paper is as follows. In Section 2, we describe the observations and the data reduction procedures; Section 3 contains color–magnitude and color–color plots and we derive the cluster reddening and metallicity; in Section 4, the RRL variable stars are presented, pulsational quantities are derived, and the distance to the cluster is determined; then we follow in Section 5 with a brief description of other variables discovered. In the final section, we present a discussion and conclusions, followed by notes on individual variables in the Appendix.

2. Observational Data and Reduction Procedures

The observations of NGC 5824 consist of 1818 calibrated CCD images from the database maintained by one of us (PBS), obtained in 26 observing runs over a period of 21 years from 1995 March until 2016 February, as listed in Table 1. The 2008–2009 CTIO 4 m Mosaic II observations were taken in time assigned for programs 2008A-0289 and 2009A-0116 to A. Walker (P.I.), and DECam time was provided similarly under program 2013A-2101. The methodologies used to produce photometry from such diverse data were similar to those used in the Homogenous Photometry series as described in detail by Stetson et al. (2014) and are based on the DAOPHOT/ALLSTAR/ALLFRAME suite of programs (Stetson 1987, 1994), which are available from P.B. Stetson. The reductions produced a catalog containing 91,779 stars[11] that tabulates the mean calibrated photometry, astrometry, and an indication of variability established using an updated version of the Welch–Stetson method (Welch & Stetson 1993) run over the individual reduced exposures.

From the 26 observing runs considered here, our data include 117 data sets obtained with *UBVRI* filters, where a data set is defined as one night's data from one CCD when the weather was photometric, or one or more night's data from one CCD when the weather was non-photometric. These observations were transformed to the Johnson–Cousins *UBVRI* system as defined by the standard stars established by Landolt (1992) by comparison of our instrumental magnitudes to the standard values provided by Stetson (catalog revision 2013 April 22). Stetson's list includes 442 stars with photometry published by Landolt (1973, 1992) also having additional observations in Stetson's archive; the listed magnitude values for these stars are the weighted average of Landolt's and Stetson's. Stetson's list also includes some 117,360 additional secondary standards, not observed by Landolt, whose observed magnitudes have been transformed to the Landolt system as described in the aforementioned papers. When we compare our derived calibrated magnitudes from those

---

Table 1
Observations

No.	ID	Dates	Telescope	Camera	No. Images	Notes
1	emmi2	1995 Mar 07–10	ESO NTT 3.6 m	EMMI	19	⋯
2	bond6	1998 Apr 16–22	CTIO 0.9 m	Tek2K3	4	⋯
3	wfi3	1999 Mar 14–19	ESO/MPI 2.2 m	WFI	80	⋯
4	wfi10:	2000 Jul 06–12	ESO/MPI 2.2 m	WFI	112	⋯
5	mzocc	2000 Jul 25–27	ESO/MPI 2.2 m	WFI	104	⋯
6	susi2a	2001 Jul 20–24	ESO NTT 3.6 m	SUSI2	30	⋯
7	wfi6	2002 Feb 18–21	ESO/MPI 2.2 m	WFI	88	⋯
8	susi03may	2003 May 30–31	ESO NTT 3.6 m	SUSI	18	⋯
9	west1	2005 Feb 11–17	CTIO 0.9 m	Tek2K3	13	a
10	B05may	2005 May 11–12	CTIO 4.0 m	Mosaic2	192	⋯
11	fors20602	2006 Feb 23–28	ESO VLT 8.0 m	FORS2	8	⋯
12	fors20605	2006 May 28–30	ESO VLT 8.0 m	FORS2	8	⋯
13	efosc08a	2008 Apr 16–28	ESO NTT 3.6 m	EFOSC	26	⋯
14	andi4	2008 Apr 17–May 14	CTIO 1.3 m	ANDICAM	63	⋯
15	may08	2008 May 02–03	CTIO 4.0 m	Mosaic2	304	⋯
16	soar08may	2008 May 02–05	SOAR 4.1 m	SOI	70	⋯
17	jul08	2008 Jul 27–29	CTIO 4.0 m	Mosaic2	8	⋯
18	aug08	2008 Aug 26–28	CTIO 4.0 m	Mosaic2	120	⋯
19	wfi46	2010 Feb 15–19	ESO/MPI 2.2 m	WFI	104	⋯
20	Y1008	2010 Aug 13–18	CTIO 1.0 m	Y4KCam	2	⋯
21	fors1103	2011 Mar 01–03	ESO VLT 8.0 m	FORS2	84	⋯
22	lee2	2011 May 29–Jun 03	CTIO 4.0 m	Mosaic2	168	a
23	D13	2013 May 05, Jul 12	CTIO 4.0 m	DECam	5	b, c
24	lcogt1	2014 Jan 19–Apr 30	Sutherland 1.0 m	CCD	88	⋯
25	D14	2014 Feb 26, Mar 08–10	CTIO 4.0 m	DECam	46	b, c
26	decam1	2016 Feb 24	CTIO 4.0 m	DECam	54	b, c

Note. (a) Strömgren filters (b) SDSS filters (c) We processed only one (in a few cases two) DECam CCDs containing the cluster.

data sets to Landolt's published values, we find root-mean-square differences of 0.025 mag per star based on 166 measurements of 14 different standards in U, 0.022 mag (759 measurements of 73 standards) in B, 0.017 mag (1452 measurements of 92 stars) in V, and 0.021 mag (488 measurements of 43 stars) in I. No measurements of Landolt's original standards were obtained in the R filter. When our calibrated magnitudes are compared to Stetson's list, we find rms differences of 0.010 mag (46,552 measurements of 5365 standards) in U, 0.011 mag (122,123 of 13,348) in B, 0.010 mag (191,569 of 15,512) in V, 0.003 mag (34,923 of 3591) in R, and 0.009 mag (124,169 of 9279) in I.

The source data include observations made in SDSS g, r, and i filters and also in Strömgren b and y filters (nos. 9 and 22 in Table 1). These were transformed to Landolt B, R, I and B, V respectively. The SDSS r and i filters are similar to the Landolt R and I bandpasses and therefore we have treated the SDSS r and i observations as if they were normal R and I observations. However, the SDSS g filter is almost exactly half-way between B and V, we chose to express SDSS g as B magnitudes plus a function of $B - V$ color, with the linear term ∼0.5 and the quadratic term ∼0.02, and then these relations were inverted to predict Landolt B from SDSS g. For non-variable stars, the prediction is quite robust with star-to-star residuals <0.02 mag. rms. However, for variable stars, the correction is applied using mean color, not instantaneous color, and, as a consequence, the mean B magnitude for a variable star predicted from SDSS g should be good, but the amplitude will be underestimated. In contrast, the Strömgren b filter is somewhat shorter than Johnson B, so transformed b-band observations will overestimate B-band amplitudes by a small amount. Conversely, Strömgren y tracks V much more closely,

with small color terms. In this paper, we discuss only the V amplitudes, and thus avoid this issue.

The cluster center is estimated to be at $(x, y) = (+9, -2)$ arcsec on our catalog coordinate system, which corresponds to R.A., decl. of $15^h03^m59^s.22$, $-33^d04^m07^s.3$, within 2–3 arcsec of the cluster center measured by Sanna et al. (2014) and Harris (1996). The center of the cluster is very crowded and we wish to produce a sub-catalog with excellent photometry that is dominated by cluster stars, for the calculation of cluster parameters and for comparison with isochrones. We therefore proceeded to make a number of selection cuts on the main catalog.

The principal issues to be considered are the photometric depth as a function of radial distance from the cluster center and the effects of crowding as the cluster center is approached. The spatial coverage is essentially complete out to a radius of 22.7 arcmin if we consider stars with at least one calibrated observation in V and also one of B or I. Coverage is partial out to (our most distant star) 33.9 arcmin. More scientifically meaningful, if we consider only stars with at least five calibrated observations in all of B, V, I, then spatial coverage is complete out to 19.6 arcmin and partial out to 32.3 arcmin. The great majority of the cluster stars are closer to the cluster center than any of these radii (see Section 3.1).

Figure 1 shows the photometric error as a function of magnitude for the B passband, and plots for the other bands are similar. The multiple sequences in the upper panel are due to the variable depth as a function of sky position, clearly demonstrating the non-homogenous nature of the data set. From plots such as these, it is straightforward to apply a cut on error as a function of magnitude, here we reject stars with errors greater than an envelope formed by limits defined at one
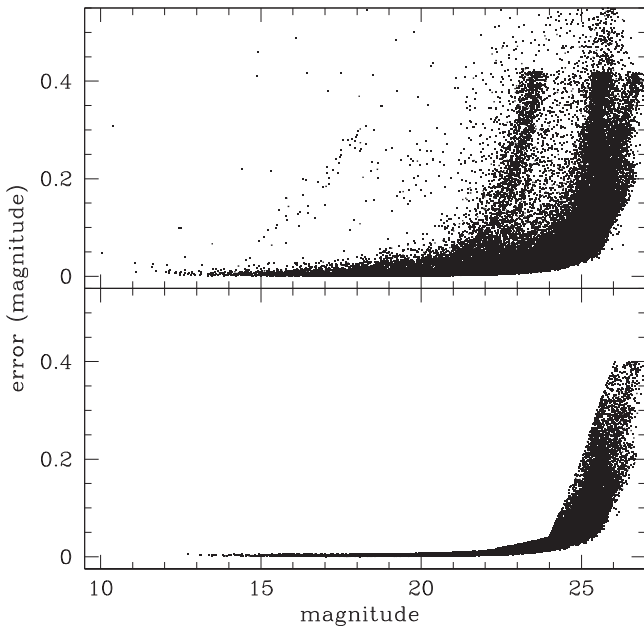
Figure 1. Photometric error as a function of magnitude for the *B*-band data. The upper panel plots all stars with *B*-band photometry, and the lower panel shows the stars remaining after the error cuts listed in Table 2.

Table 2
Error Limits in Magnitudes for Each Filter, as a Function of Magnitude

Mag.	U	B	V	R	I
10	0.005	0.005	0.005	0.005	0.005
16	0.005	0.005	0.005	0.005	0.005
17	0.006	0.005	0.005	0.005	0.005
18	0.007	0.005	0.005	0.005	0.006
19	0.010	0.006	0.007	0.005	0.008
20	0.015	0.007	0.008	0.006	0.012
21	0.03	0.009	0.01	0.01	0.02
22	0.05	0.012	0.018	0.02	0.05
23	0.10	0.025	0.03	0.05	0.10
24	0.4	0.04	0.10	0.15	0.2
25	0.4	0.2	0.4	0.4	0.4
26	0.4	0.4	0.4	0.4	0.4

rapidly brightens, suggesting that crowding errors set in abruptly at this radius. Note that the RRL, at $V \sim 18.4$, transition from the best to the poorer quality classes at a radius ~ 36 arcsec. Outside a radius ~ 900 arcsec, the quality of the photometry deteriorates slowly for most stars, and a significant fraction of the area has much shallower detection limits out to the outermost stars at ~ 2000 arcsec; this aspect is also demonstrated in Figure 1 for the *B* band.

3. The Color–Magnitude Diagram

3.1. Radial Distribution

Figure 3 shows the observed CMD for a range of eight annuli, in total extending from 1.5 to 25.5 arcmin from the cluster center. The cluster MS, which dominates in the inner annuli, is clearly still visible in the 13.5–16.5 arcmin radius panel, is just visible in the 16.5–19.5 arcmin radius panel, and is absent in the two outermost panels. The same can be said for the BHB stars. Our data out to and slightly beyond the 19.5 arcmin radius is still relatively spatially homogenous but becomes slightly photometrically shallower as radius increases (see above). For cluster RRLs confirmed to be members from their position in the CMD, we find only four more distant than a radius of 8.5 arcmin: V46 (8.63 arcmin), V26 (9.82 arcmin), V32 (12.91 arcmin), and V29 (19.32 arcmin).

As previously mentioned, since the work of Grillmair et al. (1995), the star density profile of NGC 5824 has been known to be unusual, and as shown by Carballo-Bello et al. (2012) a King model is a particularly poor fit to NGC 5824 (and to some other massive GCs in their sample), whereas a power-law fit to their data is much better, with a truncation indicated near a radius of 15 arcmin. Our data, which show the cluster MS persisting into the 16.5–19.5 arcmin radius bin would argue for a slightly greater cluster extent, but due to the non-homogenous nature of the present data set at larger radii it is not possible to significantly add to this discussion; analysis of an homogenous, deep, wide-field data set (e.g., with DECam) is out of the scope of this work but needed to make further progress. Da Costa et al. (2014) promise such an analysis.

3.2. Comparison with Isochrones

Based on the above discussion and on the experiments described in Section 2, we decided to use stars lying in an annulus centered on the cluster and with radii 90–270 arcsec to define the cluster sequences, as the best compromise between

magnitude intervals, as shown in Table 2 and with the results depicted in the lower panel of Figure 1. For all of the brighter stars, those with photometric errors greater than 0.005 mag are discarded, at the level of the cluster sub-giant branch (SGB) the error cut is still only ~ 0.01 mag. Following these cuts, the distribution of photometric error as a function of magnitude for each filter is a reasonably smooth progression. We also made cuts of the DAOPHOT photometric fitting parameters *chi* and *sharp*, to remove non-stellar objects such as galaxies, CCD defects, and unresolved double stars. We rejected objects with $sharp < -0.2$ and >0.2, and $chi < 0.7$ and >2. Given the often complex background for any given star, the discriminatory power of these parameters is less incisive than in uncrowded fields, where rather tighter limits would normally be applied, therefore these cuts can be considered supplementary to those based on the measured photometric errors. Considering only stars brighter than magnitude 22, approximately the level of the main-sequence (MS) turn-off, these cuts removed two-thirds of the *U*-band measurements and approximately half of the measurements in each of the other bands. Because this process has the side-effect of efficiently discarding variable stars, we separately add back those for which we determined periods in the plots we show below, realizing that some variables for which we do not determine periods will remain discarded, since we have no reliable way of separating them from constant stars with poor photometry. We will discuss the variable stars in detail later, so suffice it to say here that a total of 94 stars were selected as being possibly variable and thus are subject to further scrutiny.

We turn now to considering the effects of crowding, demonstrating in Figure 2 the radial zones of good photometry by plotting *V* magnitude as a function of radius, for three ranges of the error in the $B - I$ color. Similar plots are obtained for other combinations of magnitude and color. The quality of the photometry slightly improves inward to a radius of ~ 80 arcsec, due to the number of observations increasing. Inward of this radius, the magnitude limit for stars of each quality class

Table 3
Minimun Light Colors for Selected RRab Stars

Variable	Period	B min	V min	R min	I min	$E(B-V)$	$E(V-R)$	$E(V-I)$
V1	0.59725	19.372	18.768	18.451	18.036	0.231	0.046	0.151
V9	0.67762	19.379	18.777	18.327	17.926	0.210	0.180	0.272
V10	0.69472	19.271	18.750	18.343	17.888	0.124	0.137	0.283
V12	0.58008	19.392	18.872	18.467	18.076	0.151	0.134	0.215
V14	0.71077	19.181	18.644	18.307	17.901	0.136	0.067	0.163
V23	0.62808	19.373	18.872	18.359	18.031	0.120	0.244	0.261
V32	0.61479	19.314	18.738	18.375	18.028	0.199	0.093	0.129
V34	0.79620	19.156	18.577	18.202	17.724	0.158	0.105	0.273
V44	0.66460	19.319	18.651	18.312	17.875	0.279	0.070	0.197
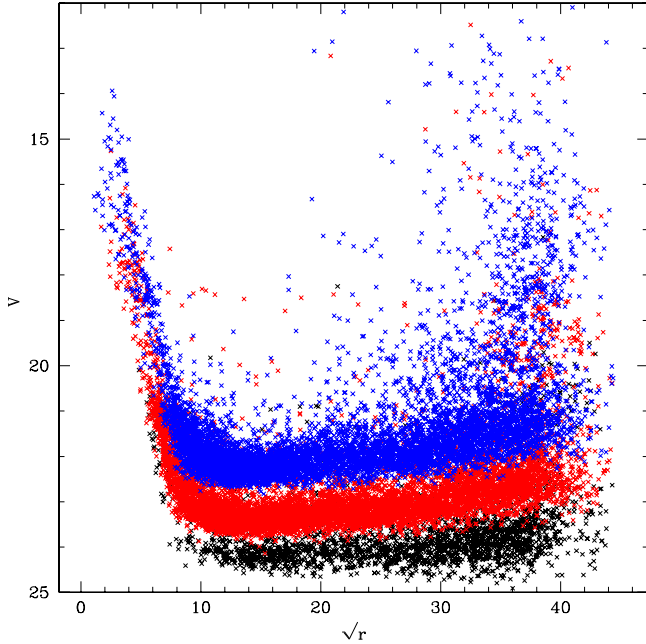
Figure 2. Plot of the V magnitude against the square root of the radial distance (arcsec) from the cluster center for stars with three ranges of error in $B - I$ color, using the original (complete) catalog as source. Color coding is: for stars with $0.09 < \sigma(B - I) < 0.10$ mag [black]; $0.03 < \sigma(B - I) < 0.04$ mag [red]; $0.01 < \sigma(B - I) < 0.015$ mag [blue].

the effects of crowding of cluster stars that strongly impacts photometry for the fainter stars for radii <90 arcsec, and the contrast of the cluster sequences against the swarm of field stars and faint unresolved galaxies at a density of ∼200 arcmin^{-2} to $V = 24$. In addition, we use the clean catalog with error cuts as shown in Table 2, and further excluded stars with errant values of DAOPHOT *chi* and *sharp* as previously described. This results in a catalog with 16,194 stars, starting from a full-field clean catalog of 83,878 stars.

The CMD of NGC 5824 has been compared to the BaSTI theoretical framework (Pietrinferni et al. 2004, 2006) in order to retrieve an estimate of the cluster age as well as an independent determination of the cluster distance and reddening. For this comparison, we adopted the α-enhanced version of the BaSTI isochrones (see Pietrinferni et al. 2006 for details). In order to perform a more detailed comparison between the empirical data set and the theoretical framework, the metallicity grid points in the original BaSTI library have been supplemented with additional stellar model computations for $Z = 0.0002$, $Y = 0.245$, and the same heavy element distribution already used for the α-enhanced BaSTI models.

These additional stellar models/isochrones are fully consistent with the original BaSTI models as far as concerns the adopted physical inputs and numerical assumptions. Comparisons between the best matching theoretical isochrones and the observed CMDs in the $(V, B - V)$ and $(V, V - I)$ photometric planes are shown in Figures 4 and 5. The best result is obtained for an apparent distance modulus equal to $(m - M)_V = 18.04$ mag and a reddening $E(B - V) = 0.15$, while the age of the isochrone that matches the MS turn-off and the SGB of the observed CMD is equal to 13 Gyr. The (internal) error in the age is ±1 Gyr.

We note that the [Fe/H] value adopted for the best matching isochrones is about 0.3 dex more metal-poor than spectroscopic measurements. Indeed, a reasonable—though slightly worse—result can be obtained by using an iron abundance about 0.15 dex larger than the value adopted for the isochrones shown in Figures 4 and 5. We think that this small mismatch between the spectroscopic measurements and the estimate based on the isochrone matching is due to a combination of uncertainty of the spectroscopic calibrations and to residual shortcomings in the color–T_{eff} relations used for transferring the stellar models from the theoretical plane to the observational ones.

The distance modulus in the comparison between the observed CMD and the theoretical models has been mainly fixed by the requirement to match the fainter boundary of the HB stellar distribution. The BaSTI models used in the present work have been computed by using the conductive opacity by Potekhin (1999). The use[12] of the most updated conductive opacities provided by Cassisi et al. (2007)—when keeping all the other physical inputs fixed—causes a decrease of the ZAHB luminosity of about $\Delta M_V \approx 0.05$–0.07 mag. It is worth noting that this shift would put the distance modulus obtained from the isochrone fitting procedure in agreement—within 1σ—with that obtained by using the period–Wesenheit relation (Section 4.2).

3.3. The Horizontal Branch and Blue Straggler Stars

We show (Figure 6) a CMD of the horizontal branch (HB) and blue straggler (BS) region of the CMD, made from the same cleaned catalog described above, but in this case extending to within 36 arcsec from the cluster center, and out to the same 270 arcsec radius, with the exception that all the identified variable stars with measured periods are plotted. Figures 4–6 all show a tight cluster turn-off region and the evolved stars sequences (SGB, RGB, AGB, HB) are all well-defined. Although the RHB

---

[12] The computation of a new release of the BaSTI theoretical framework based on the most recent physical inputs is in progress.
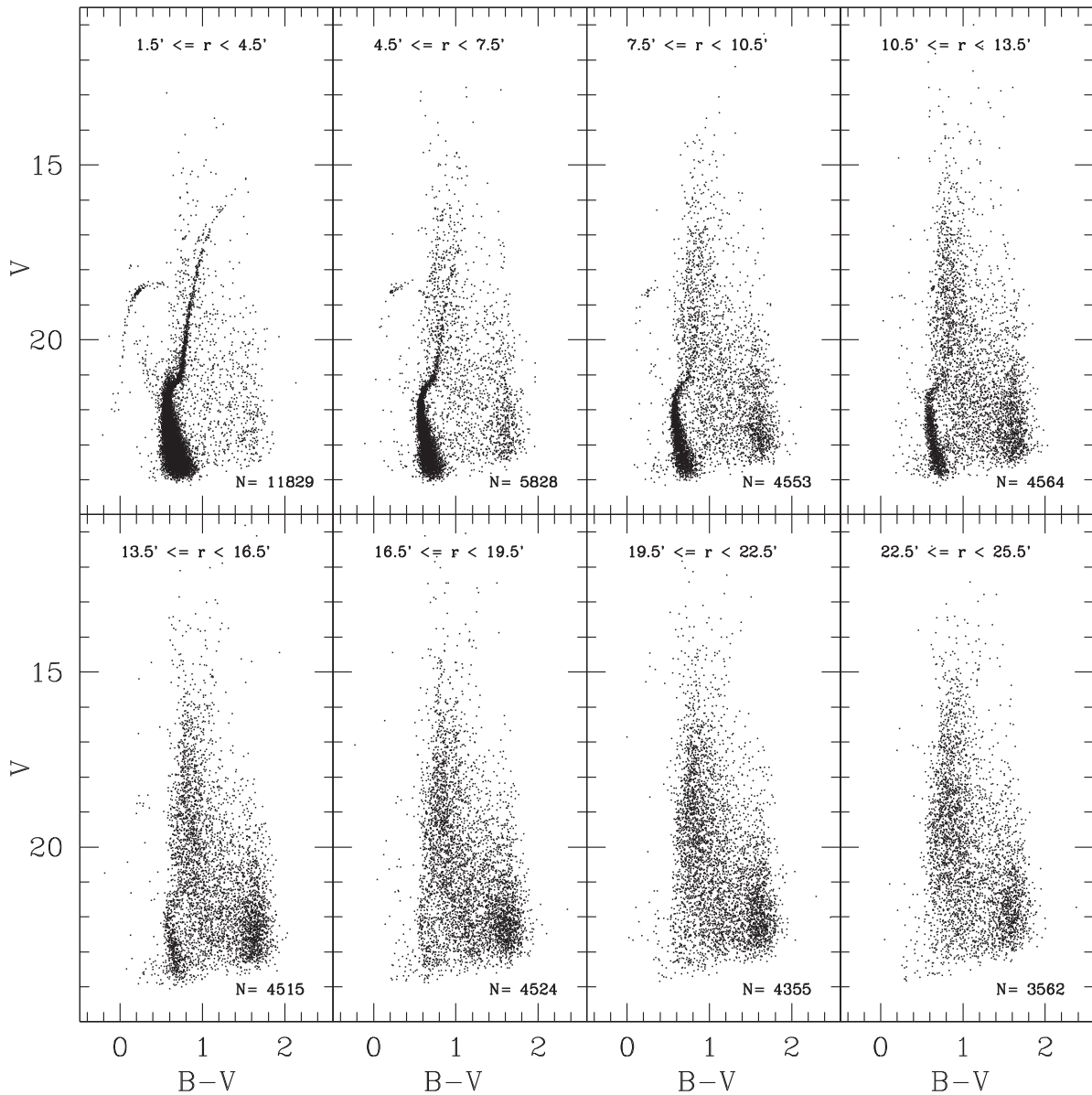
Figure 3. V, $B − V$ color–magnitude diagrams for eight annuli centered on NGC 5824, Each panel lists the inner and outer radii, and the number of stars in the figure.

area of the CMD is contaminated with field stars, there are likely a few RHB stars judging by their appearance close to the cluster center (e.g., at radii less than 60 arcsec) where most stars in the vicinity of the cluster CMD sequences statistically belong to the cluster rather than to the field.

Over a wider area, we confirm the description by Sanna et al. (2014) who show from *HST* observations in their Figure 3 that the HB extends to $m_{556} = 22$ (EHB stars), thus the HB extends beyond the so-called "Momany gap" (Momany et al. 2004) that occurs at ∼22,000 K, as commonly found in the most massive GCs. We also find, as seen in earlier studies, a prominent clump of BHB stars slightly hotter than the position of the RRL instability strip blue edge. From simple star counts using the full sample of stars with no error cuts to avoid bias when comparing to the number of RRLs, and for stars lying within the annulus with radii 36 and 270 arcsec, there are 32 RRLs, 199 ± 7 BHB stars, and 7 ± 2 RHB stars, therefore the HB descriptor introduced by Lee (1991) is $(B − R)/(B + V + R) = 0.81 ± 0.04$, where B, V, R are, respectively, the numbers of

BHB, RRL, and RHB stars. Dividing the EHB stars arbitrarily at $B − V = 0.10$, there are 40 stars bluer and 159 stars redder than this divisor. The exact evolutionary status of the hottest HB stars in GC is somewhat controversial (see, e.g., Moehler et al. 2007), with spectroscopy essential for interpretation.

We draw attention to a few stars that are bluer and/or brighter than the BHB. These are non-variables with excellent photometry and, while they may be field stars, an alternative interpretation is that they are BHB stars at the end of their helium-core burning lifetime evolving across the HR diagram to the AGB. In support of that interpretation, we also see that Sanna et al. (2014) show several supra-HB stars on their inner (*HST*) CMD where the field star contamination is low, though it is possible that some of these stars may be RRLs scattered into strange positions on the CMD due to their mean magnitudes poorly sampling the light curves. That explanation cannot be the case for the present many-epoch data set. There is also one very blue star, 69496, with $V = 19.888$, $B − V = −0.136$, $U − B = −1.001$ (see Figure 6), at position R.A. $15^h04^m09^s\!.86$, decl. $−33^d02^m07^s\!.3$ (J2000). These
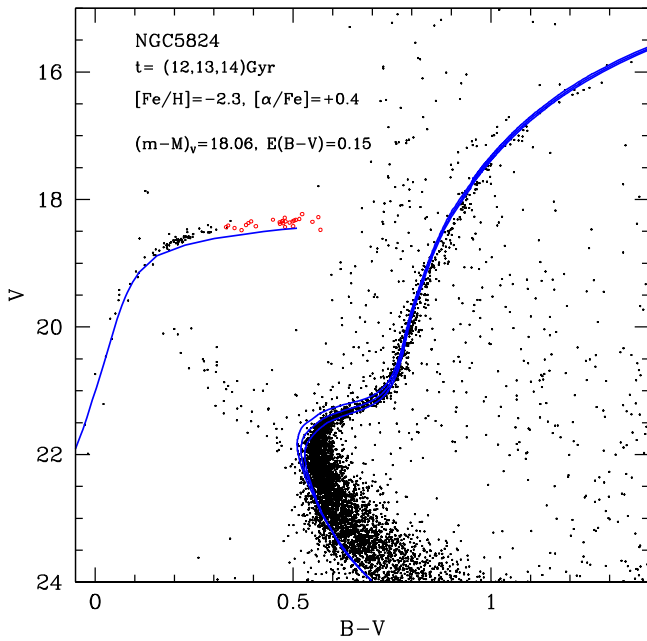
Figure 4. V, $B - V$ CMD for stars in an annulus between 90 and 270 arcsec from the center of NGC 5824. The data has stars with large errors removed, as described in the text. RRL stars are plotted as red circles. BASTI isochrones are overlaid, as specified on the figure and described in the text.
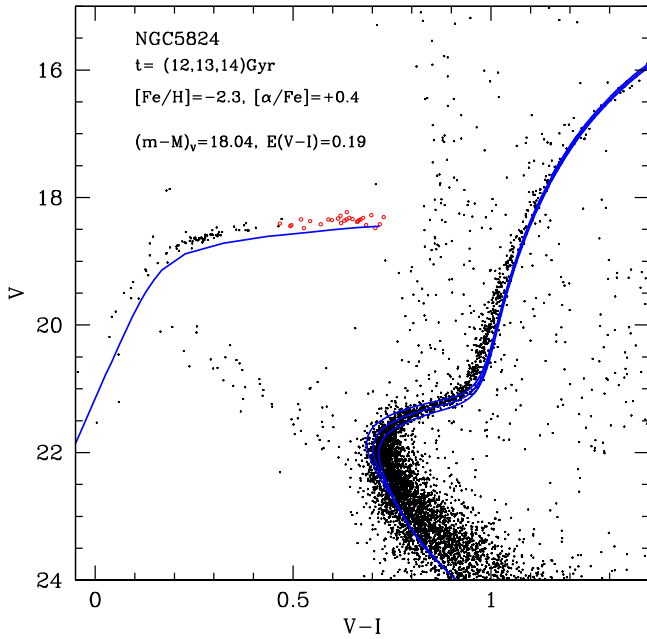

Figure 6. V, $B - V$ CMD for stars in an annulus between 36 and 270 arcsec from the center of NGC 5824. The plot is restricted to the region of the CCD in the vicinity of the horizontal branch and the blue straggler stars, with all the variable stars with measured periods plotted as filled squares, Stars with large errors have been removed, as described in the text.

Figure 5. V, $V - I$ CMD, otherwise as for Figure 4.

discuss below four SX Phe stars and an RRL star occurring among the BS stars.

3.4. Metallicity

We adopt the mean of the Da Costa et al. (2014) and Roederer et al. (2016) metallicity results, $[Fe/H] = -1.97 \pm 0.10$, noting that this is identical to earlier measurements to within the errors (Harris 1996; Carretta et al. 2009). Following techniques first introduced by Sandage & Katem (1983) and developed by Ferraro et al. (1991), we linearized the RGB in the V, $B - V$ CMD between $16 < V < 21$ by fitting a cubic polynomial, then measuring the color difference between stars and this fiducial, for stars closer to it than 0.05 mag in $B - V$ color. The distribution is approximately Gaussian with $\sigma = 0.016$ mag. If all the source of this distribution is assigned to a variation in [Fe/H], then it corresponds to $\sigma [Fe/H] = 0.10$ (Ferraro et al. 1991). This is clearly an upper limit to any metallicity spread, and we can obtain a more realistic estimate by subtracting in quadrature the photometric errors per star— remembering that we are only considering stars selected to have low photometric errors (see Table 2)—to find that the mean contribution from this source is $\sigma = 0.004$ mag. We can also expect small star to star reddening differences and general experience suggests that small-scale variations are typically at least several percent of the overall average reddening (Bellini et al. 2017), thus a variation of 5% of the reddening value would introduce $\sigma \sim 0.007$ mag. Subtracting these two sources of dispersion in quadrature leaves $\sigma = 0.006$ corresponding to $\sigma [Fe/H] = 0.05$.

3.5. Reddening

We took the catalog for the 90–270 arcsec annulus, and carefully examined the individual V, $V - I$ CMD for each quadrant, to check for differential reddening. We compared the

colors correspond closely to an unreddened DA white dwarf with $T_{eff} = 25,000$ K (Cheselka et al. 1993), and this interpretation seems the most likely. However, the star is only 3.33 arcmin from the cluster center, and the alternative explanation that it is an extremely hot cluster star evolving from the EHB requires spectroscopy for confirmation.

BS stars are prominent, as previously noted and discussed in detail by Sanna et al. (2014), with approximately 50 in the same annulus as for the HB numbers above, the uncertainty arising from the field contamination of the redder stars. We
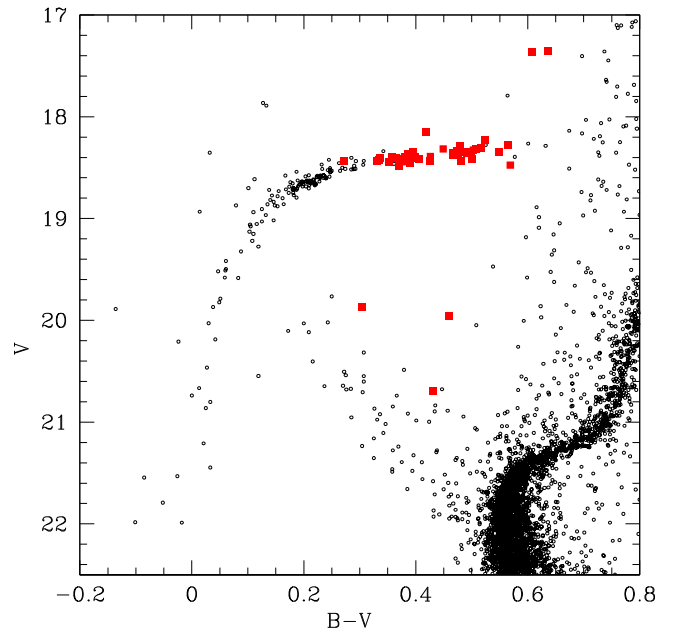
four near-vertical MS for $21.5 < V < 22.0$, for which the MS width is ~ 0.08 mag, and derived a mean color for the stars within 0.05 mag. of the MS ridgeline. The mean colors for the stars in the four photometric boxes were found to be: 0.738 ± 0.002 (NE, 287 stars), 0.736 ± 0.002 (NW, 303 stars), 0.738 ± 0.002 (SW, 292 stars), 0.740 ± 0.002 (SE, 239 stars), and similar results showing no measurable differential reddening above ~ 0.002 in $E(V - I)$ were also found when considering smaller areas within the 90–270 arcsec annulus. The NASA/IPAC dust extinction tool (http://irsa.ipac.caltech.edu/applications/DUST/) further confirms that up to a radius of ~ 10 arcmin from the center of NGC 5824 the reddening appears constant, with Schlafly & Finkbeiner (2011) finding $E(B - V) = 0.142 \pm 0.004$. We further checked by looking at the color of the lower RGB at $V = 20.0$, finding the same color in all quadrants, to conclude that any differential reddening on arcmin scales must be $\Delta E(B - V) \ll 0.01$ mag and so using a mean reddening value for stars in the 90–270 arcsec annulus is appropriate.

The actual value for the reddening can be estimated from the boundaries of the instability strip, in particular, the boundary between the BHB and the RRc stars that appears, at least in $B - V$ color, to be independent of metallicity, at $(B - V)_0 = 0.18$ (Walker 1992 & references therein). From the Figure 5 data, there is a small amount of color overlap between the reddest BHB stars and the bluest RRLs, and we estimate the boundary to be $B - V = 0.33 \pm 0.02$; therefore, $E(B - V) = 0.15 \pm 0.02$.

The reddening can also be determined from an empirical method originally developed by Sturch (1966) that uses $(B - V)$ colors for RRab variables at minimum light together with terms in period and metallicity, expressed by Walker (1990) as

$$E(B - V) = (B - V)_{min} - 0.24P - 0.056[\text{Fe}/\text{H}] - 0.336 \quad (1)$$

where the minimum light corresponds to phases between 0.5 and 0.8, period (P) is in days, and the metallicity is on the Zinn & West (1984) scale. For redder passbands, simple expressions with only the color at minimum light are adequate, with Guldenschuh et al. (2005) and Kunder et al. (2013a) finding

$$E(V - R) = (V - R)_{min} - 0.22 \quad (2)$$

and

$$E(V - I) = (V - I)_{min} - 0.58. \quad (3)$$

With $[\text{Fe}/\text{H}] = -1.97$, we then select only those RRab stars with excellent light curves (see Table 3) and measure the colors at minimum light from the fitted templates. Following Kunder et al.'s (2013a) choice of reddening law when converting from $E(V - I)$ and $E(V - R)$ to $E(B - V)$, the three colors $B - V$, $V - R$, and $V - I$ give a weighted mean of $E(B - V) = 0.15 \pm 0.03$, without including any estimate for systematic errors in the method.

Other photometric methods available here use the position of the RGB and have strong dependence on the cluster metal abundance, and thus are not as preferable to use as those discussed above, which in the mean give $E(B - V) = 0.15$, which we adopt. We can check the consistency of our adopted
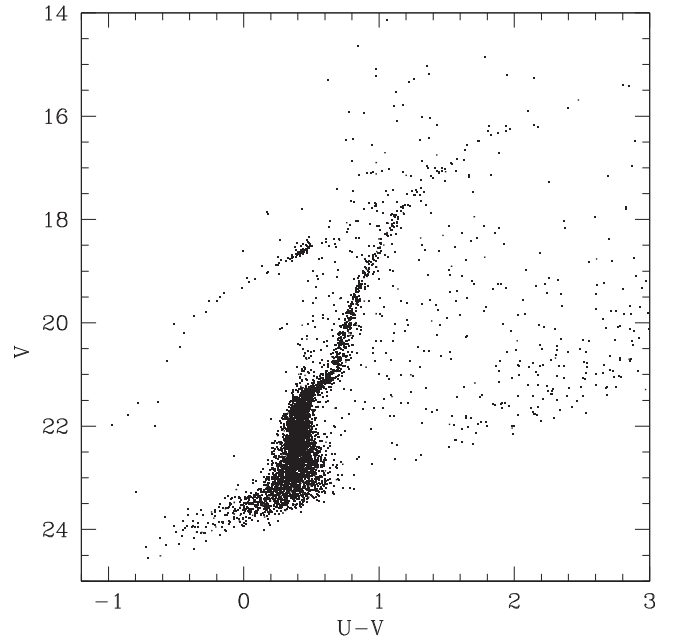

Figure 7. V, $U - V$ CMD for stars within the inner annulus (90–270 arcsec) with photometric errors less than the limits given in Table 2.

reddening and metallicity values by comparing the position and shape of the RGB relative to the HB, and with the $(B - V)_{0,g}$, $\Delta V_{1.2}$, $\Delta V_{1.1}$ relations as given by Sarajedini & Layden (1997) then with $E(B - V) = 0.15$ find $[\text{Fe}/\text{H}] = -1.84, -1.81, -1.91$, respectively, which are not far from our adopted value of $[\text{Fe}/\text{H}] = -1.97$.

3.6. Multi-populations?

We take advantage of having good photometry as deep as $U \sim 23$ to plot in Figure 7 a V, $U - V$ CMD for a cleaned sample (as described above) of stars in the 90–270 arcsec annulus centered on the cluster. Such diagrams, which include the ultraviolet, are useful for characterizing multi-population behavior (Milone et al. 2017). Specifically, we note that the SGB is narrow and cleanly defined, showing only a single sequence of stars; however, the lower RGB is very broad. All of these stars are brighter than $U = 21$ for which (Table 2) the error cut is 0.03 mag and the median error is half that. By $U = 20$, the errors are a factor of two smaller, thus photometric errors only make a minor contribution to the RGB color spread. Similarly, any contribution from differential reddening (see the discussion above) will contribute less than 0.02 mag to the color spread. We can proceed further by calculating the $c_{UBI} = (U - B) - (B - I)$ pseudo-color, which was introduced by Monelli et al. (2013) as a photometric means for identifying multiple stellar populations on the RGB of GCs. We further pre-clean the stellar sample through the use of the $B - I$ versus $U - V$ color–color diagram (Figure 8) in which the cluster RGB is clearly differentiated from the more metal-rich foreground stars (Bono et al. 2010; Monelli et al. 2013). The RGB was fitted by a polynomial of the form

$$U - V = 0.2629(B - I)^2 + 0.2406(B - I) - 0.5014 \quad (4)$$

and stars within ± 0.1 mag in $U - V$ color of the fiducial were assigned to the RGB, for $0.5 < U - V < 1.5$.

The resulting stellar sample is then plotted in the V versus c_{UBI} diagram (Figure 9), which, as shown by Monelli et al.
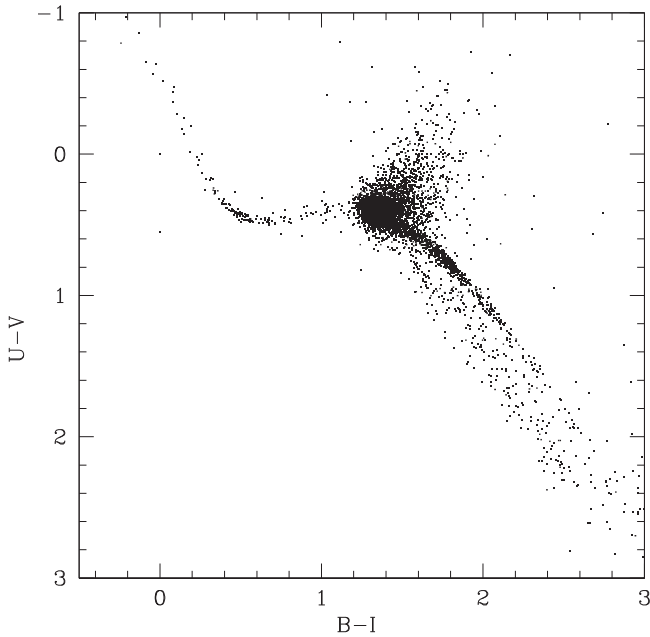
Figure 8. $B - I$, $U - V$ color–color diagram for stars within the inner annulus (90–270 arcsec). The cluster RGB on the right side of the diagram can be clearly differentiated from field stars.
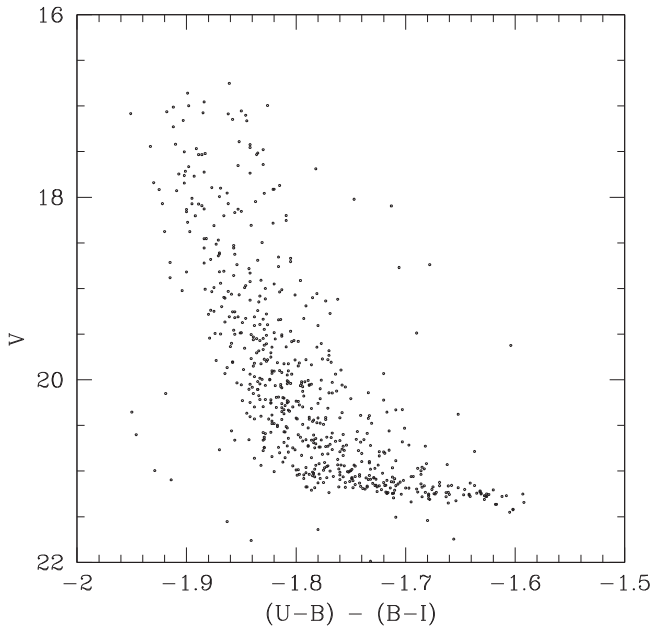

Figure 9. (V, c_{UBI}) pseudo color–magnitude diagram. The stars in this plot were selected to lie close to the cluster RGB, as shown in Figure 7, thus suppressing field stars and cluster AGB stars. Stars close to the cluster RGB tip are not included because they cannot photometrically be reliably separated from AGB stars. A bifurcation of the RGB sequence is apparent.

Figure 10. Histogram of the Δc_{UBI} parameter. This parameter is formed by first fitting a fiducial to the RGB in the (V, c_{UBI}) pseudo color–magnitude diagram (Figure 9), here we linearize with $c_{UBI} = 0.00514V^2 - 0.160V - 0.669$. Then Δc_{UBI} is formed for each star by measuring the difference between its pseudo-color and the fiducial. A multi-Gaussian fit to the histogram is also shown.

(2013), rather cleanly separates multiple populations on the RGB. Their Figure 13 shows histograms of the Δc_{UBI} parameter for 22 GC, covering a wide range of metallicity, and while for the more metal-rich and metal-intermediate clusters the separation between first and second generation (1G, 2G) stars is quite apparent, the separation for the most metal-poor clusters is less obvious. This is readily explained by the general weakening, for the metal-poor stars, of the spectral signatures that drive the pseudo-color differences (Sbordone et al. 2011; Cassisi et al. 2013). For NGC 5824, we see that the
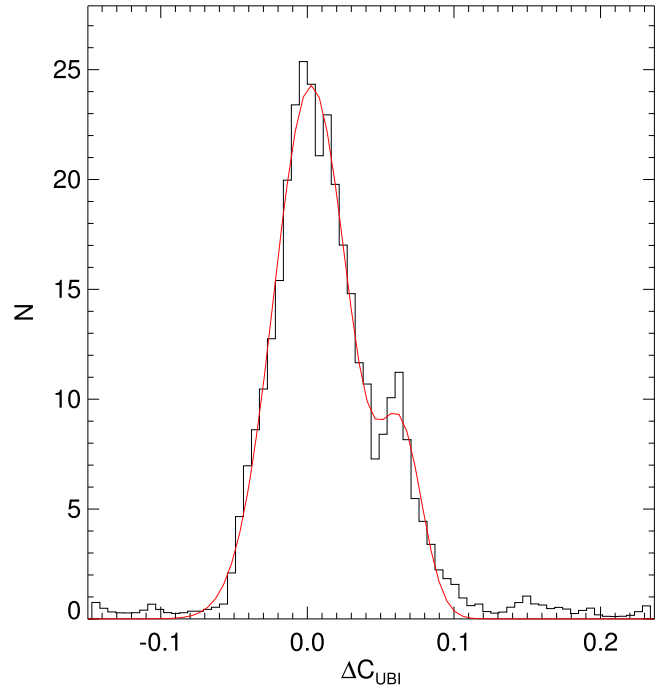
overall spread in pseudo-color for a given V magnitude is very similar to the clusters of similar metallicity (e.g., NGC 6397) shown by Monelli et al. (2013) and ascribed to a spread in light-element abundance, and the bifurcation is quite apparent. This is best demonstrated by forming the Δc_{UBI} parameter, following the procedure described by Monelli et al. (2013) and as shown in Figure 10. The main peak is populated by 1G stars, while the 2G peak is significantly less populated, the multi-Gaussian fit indicates that 75% of the stars are 1G and 25% are 2G.

It should be emphasized that all the stars plotted in Figures 9 and 10 are by selection fainter than the AGB clump (i.e., $V > 17.0$) and the color–color selection strongly removes field stars, thus this sample of RGB stars is very genuine. If we proceed to compare this result with the [Mg/Fe] distribution found by Roederer et al. (2016) for upper RGB stars we do not have such a clear-cut situation. We have deliberately excluded such stars from Figures 9 and 10 because of the difficulty of cleanly separating RGB and AGB stars, and indeed from our photometry a few of their 26 stars fall closer to the AGB sequence than to the RGB. In addition, 14 of the stars are nearer to the cluster center than our 90 arcsec cutoff, and thus contamination is a possibility, though in mitigation these are all very bright stars and photometric errors are small. Finally, we do not have U-band photometry for two stars and thus cannot compute the c_{UBI} index for these. We conclude that a comparison between the spread in [Mg/Fe] on the upper RGB and our photometry cannot be made definitively.

4. NGC 5824 RRL Variable Stars

The first variable star study of NGC 5824, by Rosino (1961), used the 74 inch telescope at the Radcliffe Observatory near

Pretoria, South Africa to discover 27 variables, all of which were classified as being of RRL type with the exception that the rather brighter V11 was stated to be of uncertain classification. From these observations, only eight stars have reliable periods, and in addition the Rosino (1961) photographic photometry has an arbitrary zeropoint. These early results are listed in the online catalog of RRLs in Galactic GCs (see Clement et al. 2001), where the positions for the NGC 5824 RRLs were determined by Samus et al. (2009).[13]

Using the method developed by Welch & Stetson (1993) and as further described by Stetson (1996), a total of 95 potential variables were flagged; of these, 57 were in the vicinity of the HB and the remainder were in the BS region of the CMD. These were examined for periodicity (see Stetson et al. 2014 for a description of the methods used) and the more difficult cases were checked multiple times using different codes and with various selections of the input data, with cuts on photometric error and the DAOPHOT parameters *chi* and *sharp*. Given the long time base and many epochs of observations, for stars with stable light curves and good photometry, it is possible to determine periods to close to one part in a million, so we quote periods to 6 decimal places in Table 4. For stars with unstable light curves, or poor photometry, or poor phase cover, we have at times had to choose one from several possible peaks in the periodogram. Such cases are noted in the Appendix, where detailed notes on the variables can be found. In addition, we have concentrated on finding short-period variables in this study and so any variable stars with periods longer than a few days (e.g., RGB variables) are likely to have been missed.

The intensity-averaged magnitudes and amplitudes were obtained by fitting the light curves with templates partly based on the set of Layden et al. (1999), following the method described in Bernard et al. (2009). The mean photometry is presented in Table 4, where stars V1-27 are those discovered and named by Rosino (1961), while the remainder are new discoveries here. An example of typical phased light curves for four variables is shown in Figure 11. The high cluster star density significantly affects the photometry for distances less than an arcmin from the cluster center, and there are likely to be unidentified RRLs inside that distance.

We have identified 47 RRLs and determined periods for 44 of them, though for two stars we consider the periods to be uncertain due to poor-quality photometry.

All 26 RRLs in the Clement et al. (2001) catalog were identified and other types of variables that were discovered are discussed below. The remaining stars in our original sample were not confirmed as periodic variables.

4.1. Oosterhoff Classification

Oosterhoff (1939) showed that the mean periods of the RRLs, and the ratio between the number of RRc and RRab variables divided clusters naturally into two groups, denoted OoI and OoII. This dichotomy, originally shown for only five clusters, is true, in general, for Galactic GC but not for clusters

in nearby galaxies, see Catelan (2009) and Braga et al. (2016) for recent discussions; thus it is interesting to see where NGC 5824 lies in this respect.

For the 42 NGC 5824 RRLs with reliable periods, 18 of these are RRab and 24 are RRc, with mean periods of 0.640 ± 0.013 (s.e) and 0.339 ± 0.008 (s.e.) days respectively. The ratio of RRc to RRab stars for a metal-poor cluster such as NGC 5824 is expected to be higher than we find; however, this is almost certainly a selection effect in that the RRab stars with high amplitudes are more likely to be discovered in the crowded central regions of the cluster than are RRc stars. This can be demonstrated by considering the number of variables found inside a radius of 1 arcmin, where we find equal numbers of each type (six each of RRab and RRc), so proportionally less RRc than at larger radii. We find only two variables inside a radius of 30 arcsec, for which crowding is severe.

Figure 12 plots the stars in the Bailey diagram. The RRLs naturally group in this diagram into the fundamental mode RRab stars and the first-overtone RRc stars. Four RRab stars (V8, V22, V40, and V49) are marked as red circles and their light curves show that these stars appear to show the Blazhko effect (Blažko 1907), which can cause the mean amplitude of the template fitted to all the data to be reduced in amplitude (see, e.g., Cacciari et al. 2005). Star V8 has a very noisy light curve, and its V amplitude may be underestimated by as much as 0.2 mag, by comparison with the B-band light curve. Stars V22 and V49 may also have amplitudes higher than shown; however, V44 has a very mild Blazhko effect, seen clearly only in the B band, with the V light curve being relatively clean. With the exception of these stars, the remainder of the RRab stars closely follows the OoII line and the scatter about the line, and the mean period is typical. Star V40 has a period of 0.53 days, which is 0.05 days shorter than the next shortest period RRab star. This star has a messy light curve and it was difficult to find the period; however, it does not display the Blazhko effect. With a V amplitude of 1.21 mag, it lies midway between the OoI and OoII fiducials in Figure 12. In summary, the RRab stars, apart from those subject to the Blazhko effect, appear to follow the OoII fiducial and there is no evidence here for a substantial OoI component among the NGC 5824 RRab variables. Many of the RRc stars in Figure 12 have poor light curves and thus are marked with red circles. Some of these stars may be double-mode (RRd) variables; however, we have not been able to determine secondary periods for any of them. The stars with good light curves (blue circles) match the fiducial shown for M22 quite well, with a displacement of ∼0.02 in log P. This may correspond to the small difference in composition between M22 and NGC 5824.

4.2. Distance

We have calculated the distance to NGC 5824 using the period–Wesenheit relations for the indices $(V, B − V)$ and $(V, B − I)$. Both relations can be considered metallicity-independent (Marconi et al. 2015; Martínez-Vázquez et al. 2015). We applied here one of the methods (so-called "theoretical," Martínez-Vázquez et al. 2015) to calculate the distance, using the two given relations applied to three different samples: RRab, RRc, and RRab+RRc, where the RRc periods have been fundamentalized by adding 0.127 to log Period (Iben 1974; Marconi et al. 2003). The estimated distance

---

[13] For V16, we find a position mismatch with that given by Clement et al. (2001), derived from Samus et al. (2009). We find that our position of R.A. 15^{h}03^{m}59^{s}31, decl. −33^{d}05^{m}08^{s}8 is 13.5 arcsec west and 7.8 arcsec south of the Samus et al. (2009) position and correctly corresponds to the star marked as V16 on Plate 1 of Rosino (1961). We find no variable star near the alternate position, and note that positions for the other 26 variables in common agree to better than a few arcsec.

Table 4
NGC 5824 Variable Stars: Periods, Photometric Parameters, and J2000 Positions

ID	Type	Period (days)	$\langle B \rangle$	$\langle V \rangle$	$\langle R \rangle$	$\langle I \rangle$	A_B	A_V	A_R	A_I	R.A. (hr:min:s)	Decl. (deg:min:s)
V1	RRab	0.597259	18.80	18.37	18.06	17.77	1.42	1.07	0.92	0.68	15 03 52.72	−33 03 35.5
V2	RRab	0.649413	18.85	18.39	18.16	17.75	1.33	1.06	0.72	0.60	15 03 59.21	−33 02 15.3
V3	RRab	0.732079	18.90	18.30	17.97	17.60	0.95	0.79	0.66	0.47	15 04 08.42	−33 03 32.6
V4	RRc	0.334383	18.80	18.40	18.14	17.86	0.66	0.41	⋯	0.28	15 04 13.47	−33 02 49.2
V5	RRab	0.630958	18.88	18.37	17.91	17.71	1.17	1.02	0.81	0.68	15 03 57.54	−33 02 20.8
V6	RRc	0.307015	18.78	18.45	18.19	17.94	0.46	0.41	0.33	0.25	15 04 06.74	−33 04 36.7
V7	RRc	0.353181	18.73	18.40	18.14	17.86	0.49	0.31	0.31	0.24	15 03 55.96	−33 05 17.8
V8	RRab	0.601377	18.93	18.40	18.18	17.74	0.78	0.69	⋯	0.42	15 03 58.09	−33 05 18.0
V9	RRab	0.677626	18.88	18.36	17.98	17.69	1.24	1.02	0.75	0.62	15 04 04.83	−33 02 53.7
V10	RRab	0.694725	18.86	18.43	18.10	17.69	0.94	0.77	0.56	0.44	15 04 11.25	−33 05 53.6
V11	Cep	2.372129	18.00	17.41	16.97	16.57	0.77	0.66	0.56	0.47	15 03 57.89	−33 04 59.8
V12	RRab	0.580085	18.88	18.43	18.13	17.79	1.51	1.21	0.95	0.72	15 03 52.90	−33 04 50.1
V13	RRc	0.3675:	18.90	18.40	18.20	17.86	⋯	⋯	⋯	⋯	15 04 00.20	−33 05 49.5
V14	RRab	0.710773	18.88	18.37	18.01	17.68	0.94	0.75	0.65	0.53	15 04 00.18	−33 03 17.4
V15	RRc	0.312907	18.79	18.46	18.20	17.96	0.45	0.37	0.39	0.25	15 04 05.28	−33 04 59.8
V16	RRc	0.390538	18.78	18.40	18.08	17.78	0.47	0.37	0.32	0.22	15 03 59.31	−33 05 08.8
V17	RRc	0.338638	18.80	18.43	18.22	17.87	0.62	0.45	0.37	0.28	15 04 01.56	−33 05 34.8
V18	RRab	0.640359	18.87	18.31	18.15	17.70	1.18	0.95	0.85	0.62	15 04 09.17	−33 04 07.6
V19	RRab	0.633701	18.78	18.22	18.00	17.61	1.15	1.01	0.83	0.58	15 03 56.41	−33 04 49.0
V20	RRc	0.398424	18.78	18.38	18.07	17.76	0.40	0.25	0.35	0.23	15 03 52.34	−33 04 30.4
V21	RRc	0.34353	18.86	18.42	18.18	17.83	⋯	⋯	⋯	⋯	15 04 02.23	−33 02 56.4
V22	RRab	0.590826	18.89	18.43	17.95	17.69	1.11	0.83	0.70	0.51	15 04 02.53	−33 04 20.3
V23	RRab	0.628086	18.96	18.43	18.08	17.76	1.18	1.04	0.70	0.67	15 03 49.59	−33 08 11.9
V24	RR	⋯	18.81	18.39	18.27	17.86	⋯	⋯	⋯	⋯	15 04 07.01	−33 09 07.5
V25	RRc	0.330884	18.82	18.49	18.23	17.96	0.63	0.50	0.43	0.29	15 03 32.38	−33 04 08.0
V26	RRab	0.592856	18.98	18.45	18.24	17.74	1.65	1.37	⋯	0.64	15 04 29.61	−32 57 53.6
V27	RRc	0.269454	18.73	18.36	18.14	17.84	0.59	0.45	0.36	0.23	15 04 24.58	−33 04 20.3
V28	EB?	⋯	20.06	19.00	⋯	17.74	⋯	⋯	⋯	⋯	15 02 33.08	−33 14 20.3
V29	RRc	0.304056	18.85	18.45	⋯	17.96	0.44	0.41	⋯	0.24	15 02 42.24	−33 05 52.4
V30	EB	0.238853	20.17	19.06	18.21	17.52	⋯	⋯	⋯	⋯	15 03 02.09	−33 01 05.7
V31	EB	0.380935	17.93	17.41	⋯	16.69	0.23	0.23	⋯	0.23	15 03 08.31	−33 19 05.2
V32	RRab	0.614798	18.86	18.40	17.72	17.72	1.20	0.95	0.81	0.72	15 03 21.63	−33 12 58.4
V33	EB?	⋯	19.78	18.76	⋯	17.31	⋯	⋯	⋯	⋯	15 03 27.58	−33 23 07.4
V34	RRab	0.796201	18.78	18.33	17.96	17.57	0.72	0.62	0.54	0.35	15 03 42.74	−33 00 55.0
V35	RRc	0.374213	18.81	18.42	18.08	17.82	0.44	0.28	0.24	0.21	15 03 48.43	−33 01 51.9
V36	RRc	0.318002	18.85	18.47	18.22	17.96	0.66	0.51	0.38	0.32	15 03 49.76	−33 06 14.0
V37	RRc	0.410966	18.86	18.34	18.08	17.78	0.58	0.26	0.25	0.26	15 03 53.46	−33 02 49.6
V38	RRc	0.315182	18.74	18.44	18.17	17.93	0.33	0.29	0.23	0.24	15 03 56.26	−33 02 54.2
V39	RR	⋯	18.88	18.27	18.16	17.57	⋯	⋯	⋯	⋯	15 03 58.35	−33 04 35.9
V40	RRab	0.530783	18.91	18.10	18.15	17.59	1.54	1.21	0.96	0.67	15 03 58.90	−33 04 33.2
V41	Cep	2.093630	17.99	17.35	16.93	16.48	0.57	0.43	0.34	0.27	15 04 00.23	−33 04 35.2
V42	RRc	0.329534	18.78	18.47	18.16	17.93	0.59	0.51	0.41	0.25	15 04 01.98	−33 06 56.1
V43	RRc	0.405010	18.89	18.39	18.40	17.79	0.34	0.15	⋯	0.16	15 04 03.55	−33 03 46.1
V44	RRab	0.664606	19.03	18.51	18.14	17.76	0.63	0.41	0.39	0.26	15 04 03.90	−33 06 57.3
V45	RRc	0.302787	18.75	18.43	18.20	17.94	0.40	0.36	0.27	0.22	15 04 16.78	−33 02 37.5
V46	RRc	0.345842	18.77	18.42	18.23	17.88	0.56	0.23	0.30	0.27	15 04 31.72	−33 07 02.5
V47	SXPhe	0.037659	19.24	18.89	⋯	18.41	0.14	0.12	⋯	0.06	15 03 04.57	−33 13 36.9
V48	RRc	0.393885	20.15	19.86	⋯	19.45	0.38	0.29	⋯	0.26	15 03 51.58	−33 17 48.2
V49	RRab	0.637410	18.85	18.26	17.95	17.48	0.85	0.41	⋯	⋯	15 03 55.88	−33 03 34.7
V50	RRc	0.380136	18.87	18.48	18.21	17.89	0.54	0.45	0.38	0.31	15 03 55.98	−33 04 09.8
V51	RRab	0.599530	18.76	18.25	17.86	17.61	1.27	1.21	1.16	0.68	15 03 56.82	−33 04 01.9
V52	RRc?	⋯	18.87	18.38	18.24	17.76	⋯	⋯	⋯	⋯	15 03 58.67	−33 03 36.8
V53	RRc	0.315564	18.55	18.19	17.99	17.66	0.51	0.30	⋯	0.12	15 04 00.62	−33 03 57.5
V54	EB?	⋯	18.52	18.09	18.14	17.49	⋯	⋯	⋯	⋯	15 04 38.20	−32 50 26.0
V55	SXPhe	0.142629	18.97	18.14	⋯	17.07	0.14	0.13	⋯	0.16	15 04 45.77	−33 12 21.2
V56	RRc	0.304147	18.69	18.33	18.13	17.78	0.41	0.37	0.29	0.20	15 03 56.45	−33 03 57.5
V57	RRc	0.314116	18.79	18.39	18.17	17.84	0.57	0.48	0.40	0.32	15 03 58.08	−33 03 37.5
V58	SXPhe	0.056937	21.12	20.69	20.41	20.13	0.31	0.29	0.18	0.13	15 03 49.59	−33 01 17.9
V59	SXPhe	0.108174	20.42	19.96	19.65	19.33	0.30	0.27	0.15	0.15	15 04 00.28	−33 05 35.8

modulus is $\mu_0 = 17.45 \pm 0.07$(systematic) ± 0.02 (random), where the mean random error per star is 0.13 mag. This corresponds to a distance of 30.9 Kpc. The fits are shown in Figure 13. There is some tension between this result and that from the isochrone matching (17.58) but formally they are just in agreement, given the errors.
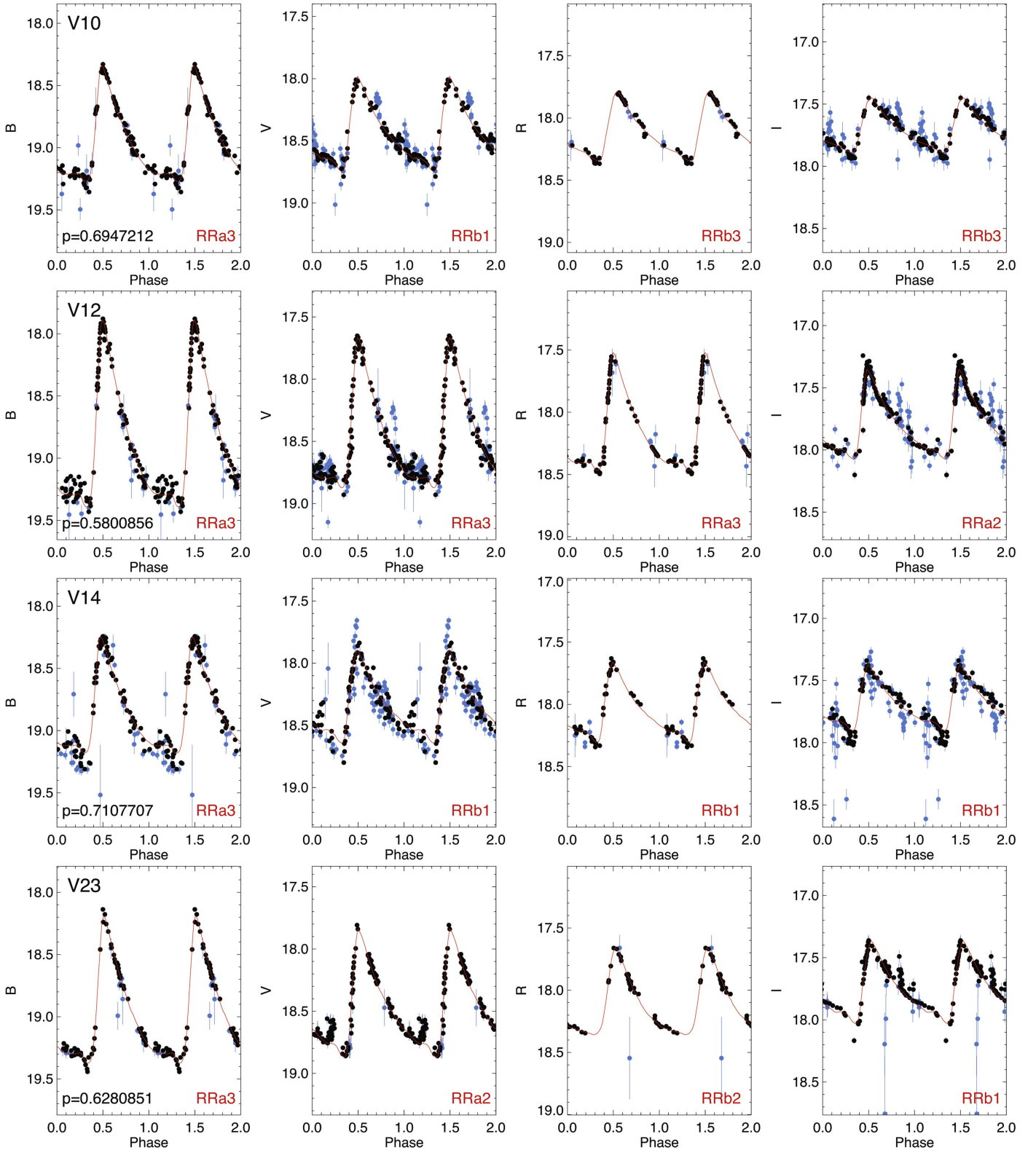
11

Figure 11. Phased *BVRI* (from left to right) light curves for the RRL stars: V10, V12, V14, and V23 (from top to bottom). The period (in days) is given in the lower-left hand corner of the left panels, the name of the star in the upper-left hand corner of the left panels and the template fits used (red curves) are shown in the lower-right hand corner of each panel. Black circles are the data points used to obtain the template fits, while blue circles show the bad data points, i.e., with errors larger than 3σ above the mean error of a given phased light curve; these were not used in the calculation of the pulsation properties.

5. Other Variable Stars

Two variable stars with periods just over two days were found lying ~1 mag above the red side of the HB (see

Figures 14, 15). Stars in this general position of the CMD, assuming they are cluster members, can be either Type II Cepheids or Anomalous Cepheids (AC). Short period (one to
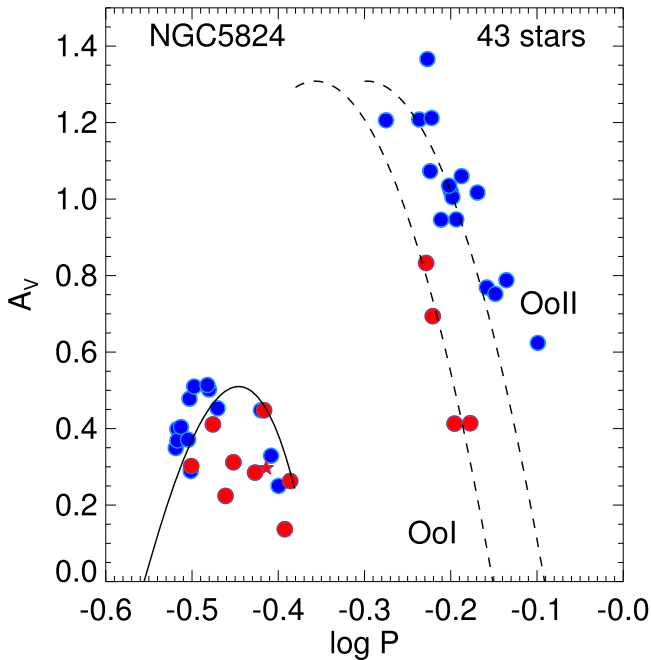
Figure 12. Bailey (or period-amplitude) diagram for the sample of RRL stars found in NGC 5824 with reliable periods (43 stars). Red circles are those stars with poor-quality light curves; some or all of these stars may be displaying the Blazhko effect (if RRab) or else be double-mode pulsators (if RRc). The star V48, which is much fainter than the HB of NGC 5824, is shown by a red star symbol. The dashed lines are the relations for RRab stars in OoI and OoII clusters obtained by Cacciari et al. (2005). The solid curve is derived from the M22 (OoII cluster) RRc variable study by Kunder et al. (2013a).

five days) Type II Cepheids are called BL Herculis stars and are rapidly evolving from the HB at the end of core-helium burning toward the AGB. The typical lifetime of a star in this phase of evolution is $\sim 8 \times 10^5$ years, about 1% of the lifetime of the HB phase (Cassisi & Salaris 2013). Thus, it is expected to find only a few such stars in a given GC, even those with a richly populated HB. The AC are metal-poor stars of one to two solar masses, and in the context of NGC 5824 they are the progeny of the blue stragglers, themselves mergers of primordial close binaries and/or products of collisions in the dense GC core. Only one AC is known in a GC (Nemec et al. 1994).

Soszyński et al. (2013) show (their Figure 3) that the light-curve shapes can be useful in discriminating between the various classes of short-period pulsating variables, and, in particular, the *I*-band light curves for BL Her stars demonstrate a characteristic rapid rise to almost maximum light followed by a rounded rather than sharp peak at maximum light. This is very similar to the light-curve shape for V11 in the redder passbands. AC light curves have a more classical saw-tooth appearance and V41, with noisier data and some phase gaps, cannot be so easily classified as V11 but may be an AC from this criterion alone. The extensive discussion of population II variables by Nemec et al. (1994) suggests that stars with periods longer than two days and luminosities ~ 3 times that for the RRL are probably Type II Cepheids and not ACs. Soszyński et al. (2013) confirm this in their Figures 5 and 6, which show the *I*-band period–luminosity (PL) relation for short-period variables in the LMC and SMC. Their plots show that only 7 out of 250 AC have periods over two days and that the luminosity separation between the two classes of variable appears to be a weak function of metallicity, important since the NGC 5824 variables are one dex more

metal-poor than the SMC average. V11 lies very close to the Type II Cepheid PL relation; however, V41, which is slightly brighter and has a shorter period, lies close to midway between the two PL relations, and thus this test cannot be considered definitive for V41. However, the rather close position of the two stars in the CMD and the presence of several supra-HB stars (see Section 3.3) would lead to the conclusion that both V11 and V41 are Type II Cepheids but that the possibility of V41 being an AC cannot be completely ruled out.

V48 (W46088) is a magnitude fainter than the cluster RRL and near the blue edge of the instability strip, it has an RRc-like light curve and a tentative period of 0.393885 days, the phased light curve is rather noisy and this period may not be the correct one. NGC 5824 variable stars in this region of the CMD would be SX Phe stars with much shorter periods. V48 is quite distant from the cluster center at 13.7 arcmin and we interpret this star as a background Galactic halo RRL with a distance modulus of 19.42 ± 0.12, ~ 77 Kpc using the same methods as described above for the cluster RRL. The most extensive sample of distant Galactic RRL candidates is found in Hernitschek et al. (2016), with stars covering a range in distance from 10 to 120 kpc, so while W46099 is more distant than most known Galactic halo RRL it is not the most distant. In any case, as pointed out by these authors and others, there are likely many more distant Galactic RRLs waiting to be discovered.

SX Phe stars in globular clusters are pulsating blue stragglers, these stars have periods much shorter than the RRL. We identify four such stars here: V47, V55, V58, and V59. SX Phe stars follow a steep PL relation (see the discussions in McNamara 2011; Fiorentino et al. 2016b), with parallel sequences for fundamental and first-overtone pulsators, and from their positions in the PL diagram it seems likely that V47 is a first-overtone pulsator and the remaining stars are pulsating in the fundamental mode.

Finally, we have determined periods for two eclipsing binaries (V30 and V31), and three other stars (V28, V33, and V54) for which we have not been able to determine periods are also likely to be eclipsing binaries. All of these stars are more distant than 17 arcmin from the center of NGC 5824 and also fall well off the cluster sequences, and thus are classified as field stars.

6. Discussion and Conclusions

Milone et al. (2017) compellingly show from high precision RGB photometry for 57 GC in bands including the vacuum-UV that 1G and 2G stars clearly separate into pseudo two-color diagrams. Unfortunately, NGC 5824 is not one of the clusters included in this study. Milone et al. (2017) further show that, although most clusters exhibit only 1G and 2G sequences, cleanly separated in their diagrams (denoted as Type I), some clusters, particularly the more massive ones, show merged or multiple 1G and/or 2G sequences (denoted as Type II). Most if not all Type II clusters also exhibit multi-sequence behavior in optical CMDs, indicative of a more complex star-formation history than the Type I clusters; for instance, NGC 1851 (Cummings et al. 2017 and references therein) has multiple SGBs indicative of C + N + O and/or He variations and complex MS, RGB, and HB sequences. Given that NGC 5824 is a rather massive cluster (see the Introduction), it is of interest to see where it fits in this scenario. The c_{UBI} diagram (Figures 9 and 10) shows that NGC 5824 has a spread in pseudo-color, with a double peak, similar to other GCs of similar low
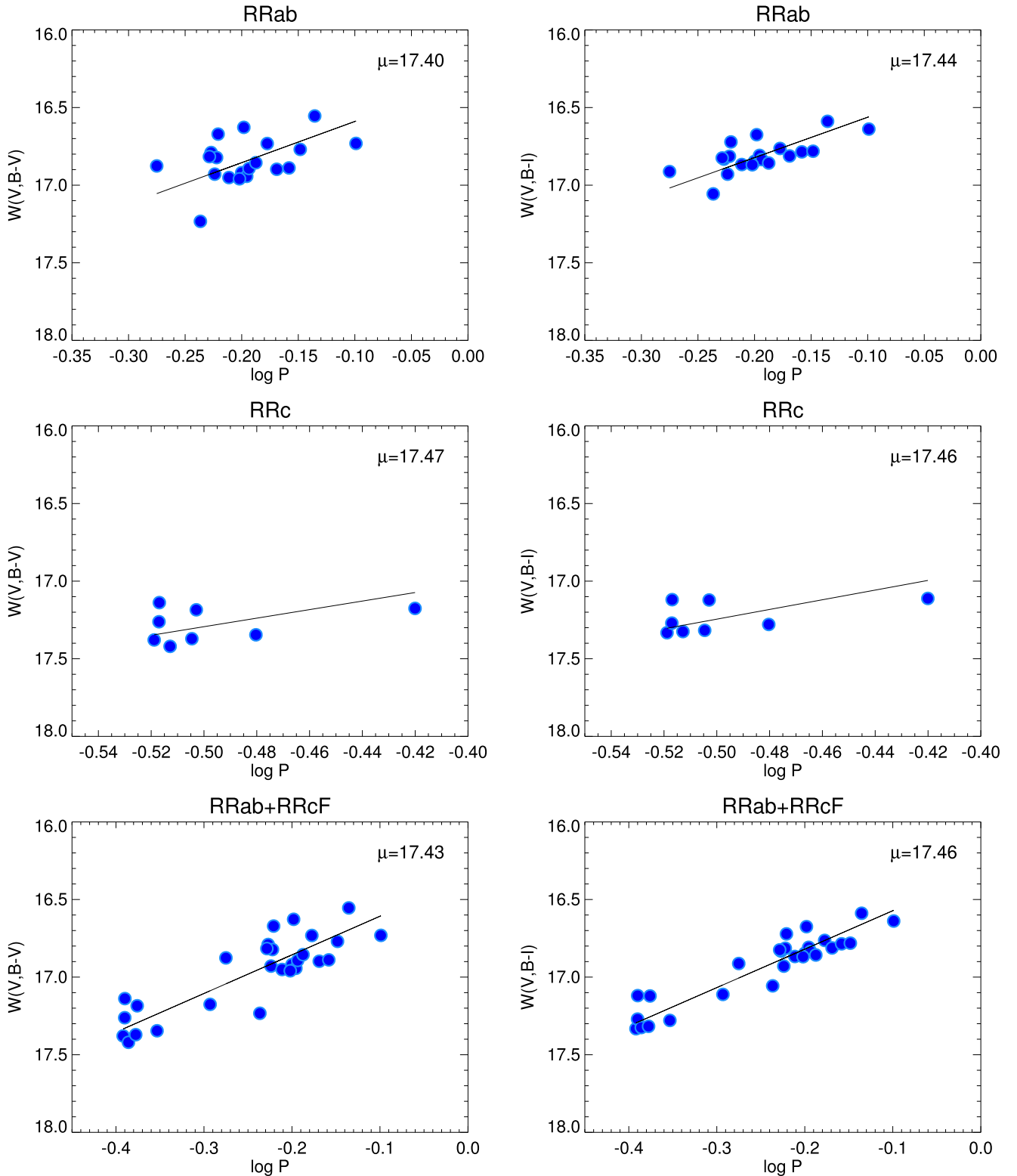
Figure 13. Apparent Wesenheit magnitudes—V, $B - V$ (left) and the V, $B - I$ (right)—vs. the logarithm of the period for the RRL stars of NGC 5824. The black lines are the theoretical period–Wesenheit relations (Marconi et al. 2015; Martínez-Vázquez et al. 2015) shifted an amount equal to the distance modulus (labeled in the upper right hand corner of each panel) derived from each subsample grouped as (from top to bottom) RRab, RRc, and RRab+RRc with periods fundamentalized (RRcF). See the text for further details.

metallicity (Monelli et al. 2013) and indicative of a mixture of 1G (75%) and 2G (25%) stars. There is no sign of other stellar populations and so this would indicate that NGC 5824 is a Type I cluster; however, precision photometry of the MS and

SGB stars with much higher spatial resolution than here—with *HST* or adaptive optics on a large ground-based telescope— would permit a stronger statement to be made. Additionally, a high-dispersion abundance study that includes the light
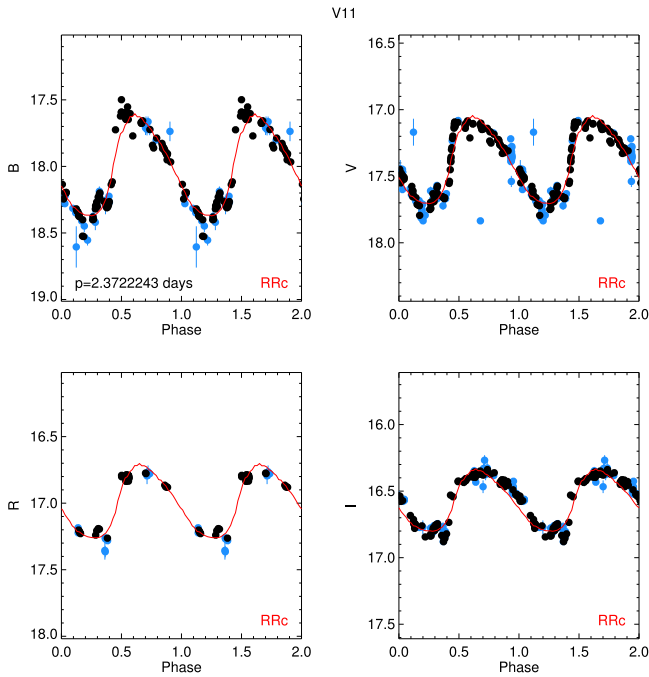
Figure 14. Phased *BVRI* light curves for the variable star V11, with a period of 2.373 days, which is a probable Type II Cepheid. See the caption of Figure 11 for details.
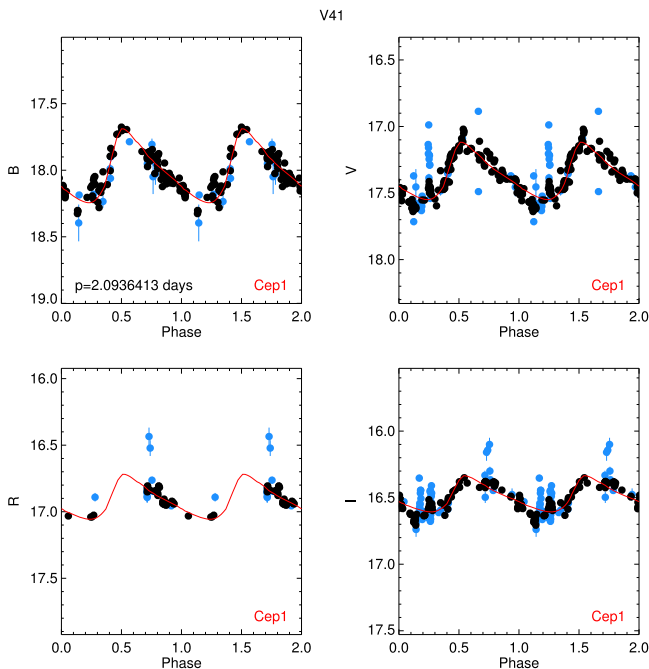
Figure 15. Phased *BVRI* light curves for the variable V41, with a period of 2.093 days, which is probably a Type II Cepheid, though classification as an Anomalous Cepheid is also possible. See the caption of Figure 11 for details.

elements (e.g., O, Na, and Al) would more clearly decipher the chemical enrichment history of the 1G and 2G stars, and indicate whether there are other star–star abundance differences that would indicate a more complex evolutionary history than the simple picture outlined here.

While the presence of RRLs is well known to indicate that an old population 10–13 Gyr is present (e.g., Walker 1989 and references therein), the pulsational properties of the variables together with the morphology of the HB can further illuminate

the star-formation history and element enrichment during that period, see, e.g., Kunder et al. (2013b), Milone et al. (2014), Martínez-Vázquez et al. (2015), and Fiorentino et al. (2016a). We show above via the Bailey diagram (Figure 12), in particular, that the RRLs define a pure OoII population with little spread in metallicity, a result that is consistent with the narrow RGB and the appearance of the HB. This evidence would further support the classification of NGC 5824 as a Type I cluster, with star formation quenched very early.

Turning now to NGC 5824's relationship with its environment, as discussed above, this study confirms earlier results but is sufficiently spatially inhomogeneous so as not to be able to make an advance on work already in the literature. While there appears to be no direct association of NGC 5824 with known stellar streams, wider and deeper surveys are showing that tidal disruption tails associated with globular clusters may be ubiquitous (Bernard et al. 2016). Although the high Galactic foreground star density makes such a detection difficult for NGC 5824, a study of the star density around the cluster on a scale of a few square degrees may be rewarding.

We conclude that NGC 5824 appears to be a relatively normal Oosterhoff Type II globular cluster and there is no evidence from this data set indicating that it had an exotic past, such as now being the remnant nucleus of a dwarf galaxy that has been completely disrupted by tidal interaction with our Galaxy.

Medioambientales y Tecnológicas-Madrid, the University of Chicago, University College London, the DES-Brazil Consortium, the University of Edinburgh, the Eidgenössische Technische Hochschule (ETH) Zürich, Fermi National Accelerator Laboratory, the University of Illinois at Urbana-Champaign, the Institut de Ciències de l'Espai (IEEC/CSIC), the Institut de Física d'Altes Energies, Lawrence Berkeley National Laboratory, the Ludwig-Maximilians Universität München and the associated Excellence Cluster Universe, the University of Michigan, the National Optical Astronomy Observatory, the University of Nottingham, the Ohio State University, the University of Pennsylvania, the University of Portsmouth, SLAC National Accelerator Laboratory, Stanford University, the University of Sussex, and Texas A&M University.

Software: DAOPHOT/ALLSTAR/ALLFRAME (Stetson 1987, 1994).

Appendix
Notes on Individual Variable Stars

Earlier work can be found in Rosino (1961) and Clement et al. (2001), who provide positions determined by Samus et al. (2009). For the new variable star discoveries (V28–V59), we include the internal identification in our catalog.

V1: Rosino (1961)'s period of 0.597 days is confirmed.
V2: Rosino (1961)'s period of 0.651 days is close to that found here. The *R*-band maximum is missing.
V3: Rosino (1961)'s period of 0.641 days is not confirmed; we find 0.732 days. Possible Blazhko star.
V4: The period is well-determined, but there is systematic scatter between the sets of observations. Possibly RRd, however, a definite secondary period could not be found. The scatter remained even after very tightly selecting the lowest error observations, and the star is not crowded.
V5: Rosino (1961)'s period of 0.634 day is confirmed. *R*-band maximum is missing.
V6: Well-defined light curve in all colors.
V7: Probable RRd given the light-curve scatter, but the secondary period was not found reliably.
V8: Noisy data Variable period? Probable Blazhko.
V9: Significant period change.
V10: Well-defined light curve.
V11: Period is 2.372 days, classified as a Type II Cepheid. The star is 1 arcmin from the cluster center.
V12: Excellent light curves in all colors. Period change visible.
V13: This star seems to have a period of about 0.3675 days, changing rapidly as a function of time. Alternative, much shorter periods seem less likely.
V14: Our period of 0.71077 days is close to double the 0.35 day tentatively found by Rosino (1961).
V15: Noisy light curve.
V16: Considerable scatter.
V17: Possible RRd?
V18: Good light curves,
V19: Blazhko?
V20: Many outliers particularly in *B* and *V*. There are alternate period possibilities.
V21: Period probably 0.343353 days, several outliers.
V22: Blazhko.
V23: Good light curves.
V24: Period possibly close to 0.33 days.

V25: Good light curves generally, more scatter in *I*.
V26: *R* band has poor phase cover.
V27: Noisy, period may be incorrect.
V28 = C7884: Probable eclipsing binary, not possible to determine the period.
V29 = C10632: No *R*-band data.
V30 = C16441: Eclipsing Binary.
V31 = C18400: Eclipsing Binary.
V32 = C22641: Good light curves.
V33 = C24689: Probable Eclipsing Binary, not possible to determine the period.
V34 = C31073: Good light curves. The longest period RRab star.
V35 = C34409: Very noisy light curve, pulsational parameters uncertain.
V36 = C35369: Some outliers.
V37 = C38462: Some outliers.
V38 = C41028: Noisy with some outliers.
V39 = C43242: Probable RRc or RRd, period not determined.
V40 = C43909: Need to select only the best data in order to find the period, definitely an RRab light curve, period of 0.530783 day is 0.05 day shorter than the next shortest period RRab star.
V41 = C45484: Period 2.09363 day, classed as Type II Cepheid. *R*-band maximum is missing.
V42 = C47656: Incomplete phase cover in *R*.
V43 = C49572: Much scatter.
V44 = C49983: Good light curves. Mild Blazhko effect seen clearly in the *B* band.
V45 = C59386: Good light curves.
V46 = C65577: Rather noisy.
V47 = W19109: SX Phe, no *R*-band data.
V48 = W46088: Fainter than the cluster RRL, no *R*-band data.
V49 = X30: Noisy, poor phase cover near maximum in all colors. Probable Blazhko.
V50 = X31: Light curve shows double sequence, probably due to blending in poor seeing.
V51 = X34: *R* band lacks maximum.
V52 = X38: Looks like an RRc, but period could not be definitively found.
V53 = X41: RRc with very noisy light curves, only *B* and *R* band are reliable. This is the closest RRL to the center of NGC 5824 (0.38 arcmin) that we have identified.
V54 = X49: Probable eclipsing binary.
V55 = X51: SX Phe.
V56 = Y2: Quite noisy.
V57 = Y24: Noisy.
V58 = SX7: SX Phe.
V59 = SX23: SX Phe.

References

Bellini, A., Anderson, J., van der Marel, R. P., et al. 2017, arXiv:1705.01951
Bernard, E. J., Ferguson, A. M. N., Schlafly, E. F., et al. 2016, MNRAS, 463, 1759
Bernard, E. J., Monelli, M., Gallart, C., et al. 2009, ApJ, 699, 1742
Blažko, S. 1907, AN, 175, 325
Bono, G., Stetson, P. B., Walker, A. R., et al. 2010, PASP, 122, 651
Braga, V. F., Stetson, P. B., Bono, G., et al. 2016, AJ, 152, 170
Brocato, E., Buonanno, R., Malakhova, Y., & Piersimoni, A. M. 1996, A&A, 311, 778
Cacciari, C., Corwin, T. M., & Carney, B. W. 2005, AJ, 129, 267

Cannon, R. D., Sagar, R., & Hawkins, M. R. S. 1990, MNRAS, 243, 151
Carballo-Bello, J. A., Gieles, M., Sollima, A., et al. 2012, MNRAS, 419, 14
Carballo-Bello, J. A., Sollima, A., Martínez-Delgado, D., et al. 2014, MNRAS, 445, 2971
Carretta, E., Bragaglia, A., Gratton, R., D'Orazi, V., & Lucatello, S. 2009, A&A, 508, 695
Cassisi, S., Mucciarelli, A., Pietrinferni, A., Salaris, M., & Ferguson, J. 2013, A&A, 554, A19
Cassisi, S., Potekhin, A. Y., Pietrinferni, A., Catelan, M., & Salaris, M. 2007, ApJ, 661, 1094
Cassisi, S., & Salaris, M. 2013, Old Stellar Populations (New York: Wiley-VCH), 197
Catelan, M. 2009, AP&SS, 320, 261
Cheselka, M., Holberg, J. B., Watkins, R., & Collins, J. 1993, AJ, 106, 2365
Clement, C., Muzzin, A., Dufton, Q., et al. 2001, AJ, 122, 2587
Cummings, J. D., Geisler, D., & Villanova, S. 2017, AJ, 153, 192
Da Costa, G. S., Held, E. V., & Savianne, I. 2014, MNRAS, 438, 3507
Ferraro, F. R., Clementini, G., Fusi Pecci, F., & Buonanno, R. 1991, MNRAS, 252, 357
Fiorentino, G., Bono, G., Monelli, M., et al. 2016a, ApJL, 798, L12
Fiorentino, G., Marconi, M., Bono, G., et al. 2016b, ApJ, 810, 15
Gratton, R. C., Carretta, E., & Bragaglia, A. 2012, A&ARv, 20, 50
Grillmair, C. J., Freeman, K. C., Irwin, M., & Quinn, P. J. 1995, AJ, 109, 2553
Guldenschuh, K. A., Layden, A. C., Wan, Y., et al. 2005, PASP, 117, 721
Harris, W. E. 1975, ApJS, 29, 397
Harris, W. E. 1996, AJ, 112, 1487
Hernitschek, N., Schlafly, E., Sesar, B., et al. 2016, ApJ, 817, 73
Iben, I., Jr. 1974, ARA&A, 12, 215
Innes, R. T. A. 1925, CiUO, 66, 328
Kinman, T. D. 1959, MNRAS, 119, 538
Kunder, A., Stetson, P. B., Cassisi, S., et al. 2013a, AJ, 146, 119
Kunder, A., Stetson, P. B., Catelan, M., Walker, A. R., & Amigo, P. 2013b, AJ, 145, 25
Landolt, A. U. 1973, AJ, 78, 959
Landolt, A. U. 1992, AJ, 104, 340
Law, D. R., & Majewski, S. R. 2010, ApJ, 718, 1128
Layden, A. C., Ritter, L. A., Welch, D. L., & Webb, T. M. A. 1999, AJ, 117, 1313
Lee, Y-W 1991, ASPC, 13, 2051
Marconi, M., Caputo, F., Di Criscienzo, M., & Castellani, M. 2003, ApJ, 596, 299
Marconi, M., Coppola, G., Bono, G., et al. 2015, ApJ., 808, 50
Martínez-Vázquez, C. E., Monelli, M., Bono, G., et al. 2015, MNRAS, 454, 1509
McNamara, D. H. 2011, AJ, 142, 110
Milone, A. P., Marino, A. E., Dotter, A., et al. 2014, ApJ, 785, 21
Milone, A. P., Marino, A. F., Piotto, G., et al. 2013, ApJ, 767, 120
Milone, A. P., Piotto, G., Renzini, A., et al. 2017, MNRAS, 464, 3636
Miocchi, P., Lanzoni, B., Ferraro, F. R., et al. 2013, ApJ, 774, 151
Moehler, S., Dreizler, S., Lanz, T., et al. 2007, A&A, 475, L5
Momany, Y., Bedin, L. R., Cassisi, S., et al. 2004, A&A, 420, 605
Monelli, M., Milone, A. P., Stetson, P. B., et al. 2013, MNRAS, 431, 2126
Nemec, J. M., Nemec, A. F. L., & Lutz, T. E. 1994, AJ, 108, 222
Newbury, H. J., Yanny, B., & Willett, B. A. 2009, ApJL, 700, L61
Oosterhoff, P. T. 1939, Obs, 62, 104
Pawlowski, M. S., Pflamm-Altenburg, J., & Kroupa, P. 2012, MNRAS, 423, 1109
Pietrinferni, A., Cassisi, S., Salaris, M., & Castelli, F. 2004, ApJ, 612, 168
Pietrinferni, A., Cassisi, S., Salaris, M., & Castelli, F. 2006, ApJ, 642, 797
Pietrinferni, A., Cassisi, S., Salaris, M., & Hidalgo, S. 2013, A&A, 558, A46
Piotto, G. 2009, in IAU Symp. 258, ed. E. E. Mamajek, D. R. Soderblom, & R. F. G. Wyse (Cambridge: Cambridge Univ. Press), 233
Piotto, G., King, I. R., Djorgovski, S. G., et al. 2002, A&A, 391, 945
Potekhin, A. Y. 1999, A&A, 351, 787
Renzini, A., D'Antona, F., Cassisi, S., et al. 2015, MNRAS, 454, 4197
Roederer, I. U., Mateo, M., Bailey, J. I., III, et al. 2016, MNRAS, 455, 2417
Rosino, L. 1961, PASP, 73, 309
Samus, N. N., Kszarovets, E. V., Pastukhova, E. N., Tsvetkova, T. M., & Durlevich, O. V. 2009, PASP, 121, 1378
Sandage, A., & Katem, B. 1983, AJ, 88, 1146
Sanna, N., Dalessandro, E., Ferraro, F. R., et al. 2014, ApJ, 78, 90
Sarajedini, A., & Layden, A. 1997, AJ, 113, 264
Sbordone, L., Salaris, M., Weiss, A., & Cassisi, S. 2011, A&A, 534, A9
Schlafly, E. F., & Finkbeiner, D. P. 2011, ApJ, 737, 103
Soszyński, I., Udalski, A., Szymański, M. K., et al. 2013, AcA., 65, 233
Stetson, P. B. 1987, PASP, 99, 191
Stetson, P. B. 1994, PASP, 106, 250
Stetson, P. B. 1996, PASP, 108, 851
Stetson, P. B., Braga, V. F., Dall'Oro, M., et al. 2014, PASP, 121, 521
Sturch, C. 1966, ApJ, 143, 774
Walker, A. R. 1989, PASP, 101, 570
Walker, A. R. 1990, AJ, 100, 1532
Walker, A. R. 1992, ApJ, 390, L81
Welch, D. L., & Stetson, P. B. 1993, AJ, 105, 1813
Zinn, R. 1985, ApJ, 293, 424
Zinn, R., & West, M. J. 1984, ApJS, 55, 45